

Seasonal Water Mass Evolution and Non-Redfield Dynamics Enhance CO₂ Uptake in the Chukchi Sea

Key Points:

- Atmospheric CO₂ uptake potential is larger in the nutrient-rich non-Alaska Coastal Water than the nutrient-poor Alaska Coastal Water
- For the most intensive growing period (spring to early summer), net community production estimation was 66%–84% higher based on dissolved inorganic carbon (DIC) than NO₃⁻
- A non-Redfield C:N uptake ratio by phytoplankton enables more efficient DIC-fixation and contributes 30%–46% of CO₂ uptake

Supporting Information:

Supporting Information may be found in the online version of this article.

Correspondence to:

W.-J. Cai,
wcai@udel.edu

Citation:

Ouyang, Z., Collins, A., Li, Y., Qi, D., Arrigo, K. R., Zhuang, Y., et al. (2022). Seasonal water mass evolution and non-Redfield dynamics enhance CO₂ uptake in the Chukchi Sea. *Journal of Geophysical Research: Oceans*, 127, e2021JC018326. <https://doi.org/10.1029/2021JC018326>

Received 7 DEC 2021

Accepted 1 JUL 2022

Author Contributions:

Conceptualization: Zhangxian Ouyang, Wei-Jun Cai

Data curation: Zhangxian Ouyang, Andrew Collins

Formal analysis: Zhangxian Ouyang

Funding acquisition: Yun Li, Wei-Jun Cai

Investigation: Di Qi, Kevin R. Arrigo, Yanpei Zhuang, Shigeto Nishino, Matthew P. Humphreys, Naohiro Kosugi, Akihiko Murata

Methodology: Zhangxian Ouyang

Resources: Liqi Chen, Jianfang Chen

Zhangxian Ouyang¹ , Andrew Collins^{1,2}, Yun Li¹, Di Qi^{3,4} , Kevin R. Arrigo⁵ , Yanpei Zhuang^{3,6}, Shigeto Nishino⁷ , Matthew P. Humphreys⁸ , Naohiro Kosugi⁹ , Akihiko Murata¹⁰ , David L. Kirchman¹, Liqi Chen⁴ , Jianfang Chen⁶ , and Wei-Jun Cai¹

¹School of Marine Science and Policy, University of Delaware, Newark, DE, USA, ²NOAA Pacific Marine Environmental Laboratory, Seattle, WA, USA, ³Polar and Marine Research Institute, Jimei University, Xiamen, China, ⁴Key Laboratory of Global Change and Marine-Atmospheric Chemistry of Ministry of Natural Resources, Third Institute of Oceanography, MNR, Xiamen, China, ⁵Department of Earth System Science, Stanford University, Stanford, CA, USA, ⁶Key Laboratory of Marine Ecosystem Dynamics, Second Institute of Oceanography, Ministry of Natural Resources, Hangzhou, China, ⁷Institute of Arctic Climate and Environment Research, Japan Agency for Marine-Earth Science and Technology (JAMSTEC), Yokosuka, Japan, ⁸Department of Ocean Systems (OCS), NIOZ Royal Netherlands Institute for Sea Research, Texel, The Netherlands, ⁹Meteorological Research Institute, Tsukuba, Japan, ¹⁰Global Ocean Observation Research Center, Research Institute for Global Change, Japan Agency for Marine-Earth Science and Technology (JAMSTEC), Yokosuka, Japan

Abstract The Chukchi Sea is an increasing CO₂ sink driven by rapid climate changes. Understanding the seasonal variation of air-sea CO₂ exchange and the underlying mechanisms of biogeochemical dynamics is important for predicting impacts of climate change on and feedbacks by the ocean. Here, we present a unique data set of underway sea surface partial pressure of CO₂ (*p*CO₂) and discrete samples of biogeochemical properties collected in five consecutive cruises in 2014 and examine the seasonal variations in air-sea CO₂ flux and net community production (NCP). We found that thermal and non-thermal effects have different impacts on sea surface *p*CO₂ and thus the air-sea CO₂ flux in different water masses. The Bering summer water combined with meltwater has a significantly greater atmospheric CO₂ uptake potential than that of the Alaskan Coastal Water in the southern Chukchi Sea in summer, due to stronger biological CO₂ removal and a weaker thermal effect. By analyzing the seasonal drawdown of dissolved inorganic carbon (DIC) and nutrients, we found that DIC-based NCP was higher than nitrate-based NCP by 66%–84% and attributable to partially decoupled C and N uptake because of a variable phytoplankton stoichiometry. A box model with a non-Redfield C:N uptake ratio can adequately reproduce observed *p*CO₂ and DIC, which reveals that, during the intensive growing season (late spring to early summer), 30%–46% CO₂ uptake in the Chukchi Sea was supported by a flexible stoichiometry of phytoplankton. These findings have important ramification for forecasting the responses of CO₂ uptake of the Chukchi ecosystem to climate change.

Plain Language Summary The Chukchi Sea has been suggested to take more CO₂ from the atmosphere as a result of decreased sea ice coverage and increased inflow of nutrient-rich Pacific Water. In order to better understand the seasonal variations in CO₂ uptake and net community production (NCP) on the Chukchi shelf, we examined the data of sea surface partial pressure of CO₂ and biogeochemical properties collected in five consecutive cruises from spring to fall in 2014. We found that the nutrient-rich Bering Summer Water combined with meltwater has a larger CO₂ uptake potential than that of the nutrient-poor Alaska Coastal Water. In addition, we estimated NCP based on the seasonal drawdown of dissolved inorganic carbon and nutrients, and found that NCP derived from carbon deficit was consistently higher than NCP derived from NO₃⁻. We attributed this inconsistency to a high C:N uptake ratio because phytoplankton growth may not always follow the canonical Redfield ratio. With a model simulation, we further quantified that this non-Redfield C:N uptake in phytoplankton enables more efficient carbon-fixation and contributes 30%–46% CO₂ uptake from atmosphere during the intensive growing season in the Chukchi Sea.

© 2022. The Authors.

This is an open access article under the terms of the [Creative Commons Attribution License](https://creativecommons.org/licenses/by/4.0/), which permits use, distribution and reproduction in any medium, provided the original work is properly cited.

1. Introduction

As the first region of the Arctic Ocean to receive water and nutrient inputs from the Pacific Ocean, the Chukchi Sea is a unique ecosystem affecting Arctic biogeochemical cycles, food-web function, and air-sea CO₂ fluxes (Bates et al., 2011; Grebmeier et al., 2015; Tremblay et al., 2015). The high biological productivity and the

Writing – original draft: Zhangxian Ouyang, Andrew Collins, Wei-Jun Cai
Writing – review & editing: Zhangxian Ouyang, Andrew Collins, Yun Li, Di Qi, Kevin R. Arrigo, Yanpei Zhuang, Shigeto Nishino, Matthew P. Humphreys, Naohiro Kosugi, Akihiko Murata, David L. Kirchman, Liqi Chen, Jianfang Chen, Wei-Jun Cai

associated strong CO₂ sink of the Chukchi Sea are primarily sustained by northward flowing, nutrient-rich Pacific Water (Ardyna & Arrigo, 2020; Lewis et al., 2020; Ouyang et al., 2020; Tu et al., 2021). Woodgate (2018) reported that the annual mean flow of Pacific Water has increased by ~50% between 1990 and 2015, bringing much more nutrients onto the Chukchi shelf, which has led to higher primary production and CO₂ uptake in recent decades (Arrigo and van Dijken, 2015; Lewis et al., 2020). However, the increase of the annual mean transport of different water masses is not proportional (Woodgate, 2018), which implies that the Chukchi ecosystem may respond differently to the volume increase depending on the different properties of the incoming waters. For example, Lowry et al. (2015) suggested that the summer phytoplankton bloom was sustained by the nutrient-rich winter water and that the persistent biological “hotspot” in the northern Chukchi Sea was driven by the flow and confluence of Pacific winter water rather than the summer Alaska Coastal Water (ACW). This was corroborated by a recent model study (Zheng et al., 2021). Counterintuitively, Strong et al. (2016) found that carbon export was larger in the less-productive ACW than in other more productive water masses. Thus, possible changes of water masses and related changes in water column structure may, in return, affect biogeochemical processes in the Chukchi Sea.

In addition, the seasonal evolution of water masses associated with variations in biological processes plays a key role in controlling nutrients and carbon cycles in the Chukchi Sea. High primary production associated with Pacific Water inflow and sea ice retreats transforms the Chukchi Sea from a nutrient-rich system in spring to a nutrient-limited system in summer (Mills et al., 2015; Zhuang et al., 2020). Such a substantial change in nutrient availability potentially changes the uptake ratio of nutrients and carbon by phytoplankton to form particulate organic matter (POM) and dissolved organic matter (DOM) during primary production and complicates our understanding of the seasonal net community production (NCP) and CO₂ uptake from the atmosphere in the Chukchi Sea (Tu et al., 2021; Zheng et al., 2021). Deviations of C:N uptake stoichiometry from the Redfield ratio have been widely observed over the world's oceans (Koeve, 2006; Martiny et al., 2013; Park et al., 2008). Several model studies have suggested that non-Redfield stoichiometry of phytoplankton should be taken into account to better project the net primary production, food quality and ocean carbon uptake in response to climate change (Buchanan et al., 2018; Kwiatkowski et al., 2018). However, a variable C:N uptake stoichiometry within a seasonal scale is rarely investigated and it is much less known how a non-Redfield C:N assimilation ratio of phytoplankton may affect NCP and CO₂ uptake in a climate-sensitive region such as the Chukchi Sea.

As the Chukchi Sea is one of the fastest changing regions in the world due to anthropogenic climate changes (Lewis et al., 2020; Meredith & Sommerkorn, 2019; Onarheim et al., 2018; Stroeve & Notz, 2018; Woodgate & Peralta-Ferriz, 2021), it is important to better understand the fundamental drivers, causes, and patterns in seasonal biogeochemical dynamics. Although many efforts have been made to demonstrate the seasonal variation in CO₂ fluxes and biogeochemistry in the Chukchi Sea (Ardyna & Arrigo, 2020; Lowry et al., 2015; Ouyang et al., 2021; Zheng et al., 2021), most of them were based on observations that were either within a single season or over multiple seasons across different years. Given that sea ice conditions in the Chukchi Sea vary from year to year, the timing and magnitude of physical and biological processes change correspondingly, perhaps causing a large uncertainty in deconvoluting the complicated relationship between seasonal air-sea CO₂ flux, NCP, and carbon and nutrient consumption using data collected across different years. Therefore, measurements of biogeochemical properties across multiple periods within a single year provide us a great opportunity to elucidate the links between seasonal evolution of water masses and the associated biogeochemical processes and ecosystem responses, which are essential for forecasting the responses of the Chukchi ecosystem to climate change.

Here, we present a data set of underway sea surface temperature (SST), salinity (SSS) and sea surface CO₂ partial pressure (*p*CO₂) measured in five consecutive cruises in the Chukchi Sea from spring to fall in 2014 (Table 1). We take advantage of this unique data set to examine both the spatial and seasonal variations in sea surface *p*CO₂, and then explore the dominant drivers of seasonal *p*CO₂ change along water mass evolution. We also use discrete sample-based biogeochemical properties including DIC, total alkalinity (TA), nutrients (NO₃⁻ and PO₄³⁻), dissolved oxygen (DO), and chlorophyll *a* (Chl *a*) from three cruises to identify how seasonal evolution of water masses affect biogeochemical dynamics. In addition, we calculated NCP based on seasonal changes in DIC and nutrients and discussed possible mechanisms for the observed inconsistency in the derived NCP values. Finally, we used a box model to evaluate the impacts of non-Redfield C:N uptake by phytoplankton on seasonal CO₂ uptake in the Chukchi Sea.

Table 1
Summary of Cruises Information and Data Sources

Cruise	Period	Vessel	Data source of sea surface $p\text{CO}_2$	Data source of discrete samples
33HQ20140505	Start: 5 May 2014 End: 21 June 2014	Healy, USA	SOCATv2020	https://arcticdata.io/catalog/view/doi%3A10.18739%2FA21C1TG6R
33HQ20140709	Start: 9 July 2014 End: 2 August 2014	Healy, USA	SOCATv2020	No data collected
33HQ20140810	Start: 10 August 2014 End: 29 August 2014	Healy, USA	SOCATv2020	No data collected
76XL20140727	Start: 27 July 2014 End: 9 September 2014	Xuelong, China	SOCATv2020	https://data.mendeley.com/datasets/dfpxwm24c/2
49NZ20140831	Start: 3 September 2014 End: 28 September 2014	Mirai, Japan	JAMSTEC	http://www.godac.jamstec.go.jp/darwin/cruise/mirai/mr14-05/e

2. Method

2.1. Study Area and Water Masses

The water mass properties and circulation in the Chukchi Sea have been extensively studied and presented in many previous works (Corlett & Pickart, 2017; Gong & Pickart, 2015; Li et al., 2019; Lin et al., 2019; Pacini et al., 2019; Pickart et al., 2019; Stabeno et al., 2018). Briefly, three main current branches of Pacific Water flow northward through Bering Strait onto the Chukchi Sea shelf (Figure 1). On the eastern side, the ACW branch flows along the Alaskan coast toward Barrow Canyon (known as the Alaskan Coastal Current (ACC) in summer and fall). The central branch flows through Central Channel between Herald Shoal and Hanna Shoal (Weingartner



Figure 1. Schematic circulation of the Chukchi Sea and the names of associated geographical locations (after Corlett & Pickart, 2017).

Table 2
Definition of Water Masses in the Chukchi Sea

Water masses		Temperature (°C)	Salinity
Newly-ventilated Winter Water	NVWW	$T < -1.6^{\circ}\text{C}$	$S > 31.5$
Remnant Winter Water	RWW	$-1.6^{\circ}\text{C} < T < 0^{\circ}\text{C}$	$S > 31.5$
Alaskan Coastal Water	ACW	$T > 3.0^{\circ}\text{C}$	$30 < S < 32$
Bering Summer Water	BSW	$0^{\circ}\text{C} < T < 3.0^{\circ}\text{C}$	$30 < S < 33.6$
		$T > 3.0^{\circ}\text{C}$	$32 < S < 33.6$
Early-season Melt Water	ESMW	$T < 0^{\circ}\text{C}$	$S < 31.5$
Late-season Melt Water	LSMW	$T > 0^{\circ}\text{C}$	$S < 30$
River Water	RW	$T > 8.0^{\circ}\text{C}$	$S < 30$

et al., 2005; Woodgate & Aagaard, 2005). The western branch transports Anadyr Water along the Siberian coast toward Herald Canyon (Weingartner et al., 2005). However, there is increasing evidence that the flows are not as rigidly confined to these three separate pathways as was originally thought. For example, a portion of western branch flows eastward to the north of Herald Shoal, where it meets the central branch before joining the eastern branch and exiting the shelf via Barrow Canyon (Figure 1). It is evident that topographic features such as canyons and shoals greatly affect the shelf circulation.

To focus on the Chukchi shelf, data used for this study were limited from 66°N to 74°N to a maximum of 120 m to exclude deep waters from the Canada Basin. We adopted the water mass classification used by several previous studies (Table 2; Corlett and Pickart et al., 2017; Gong & Pickart, 2015; Pacini et al., 2019; Pickart et al., 2019; Wang et al., 2022). The coldest water is known as Newly-Ventilated Winter Water (NVWW; $T < -1.6^{\circ}\text{C}$), which is typically observed from spring to early-summer over the entire shelf. As summer progresses, this winter water can be converted to Remnant Winter Water (RWW; $-1.6^{\circ}\text{C} < T < 0^{\circ}\text{C}$) by solar heating or mixing with warmer summer water, which sometimes lasts into summer (Gong & Pickart, 2015). During summer and early fall, the Chukchi Sea mainly contains two Pacific summer waters. The first is ACW, which originates in the Gulf of Alaska. In the summer, the ACC carries predominantly ACW in the eastern Chukchi Sea, in which the water temperature can reach $>10^{\circ}\text{C}$. The second is a combination of Anadyr Water and central Bering Shelf water, which is referred to as Bering Summer Water (BSW). The seasonal sea ice Melt Water (MW) forms a layer of fresh water on the Chukchi shelf. Sometimes it can also be divided into early-season melt water and late-season melt water (Table 2; Gong & Pickart, 2015; Pickart et al., 2019). This freshwater layer evidently occupies a large portion of the Chukchi/Beaufort shelfbreak regions in the mid-to late-summer. In these regions, the densest and saltiest water, the Atlantic Water (AW; $T > -1.0^{\circ}\text{C}$ and $S > 33.6$), can be observed at depths below ~ 150 m, but it is rarely observed on the Chukchi shelf. However, AW can be upwelled occasionally through Barrow Canyon (Pisareva et al., 2019) and Herald Canyon (Pickart et al., 2010).

2.2. Underway Measurements

It is unusual that there are five survey cruises in 1 year (2014) with underway sea surface temperature (SST), salinity (SSS) and $p\text{CO}_2$ measured in the Chukchi Sea (Table 1). To our knowledge, this is the only year so far with such high-density observations. The underway data were obtained from the SOCAT database (v2020; Bakker et al., 2016) and Japan Agency for Marine-Earth Science and Technology (JAMSTEC) (Table 1). Specifically, the underway SST and SSS were measured using an underway water monitoring system in an intake port near the bow of the ships (5–7 m below the waterline). The underway sea surface $p\text{CO}_2$ from USCGC Healy and RV Xuelong was measured using an underway $p\text{CO}_2$ system (General Oceanic, USA) described in Pierrot et al. (2009). The data from RV Mirai was analyzed by a Greenhouse Gas Analyzer (Los Gatos Research, USA). These systems were monitored and calibrated with four certified gas standards (NOAA) every 2–3 hr. The overall precision of the reported sea surface $p\text{CO}_2$ values was estimated to be $\pm 2 \mu\text{atm}$. The underway $p\text{CO}_2$ system and data reduction procedure were described by Pierrot et al. (2009).

2.3. Discrete Sample Analysis

Discrete biogeochemical samples were collected during three cruises (Table 1). The datasets of discrete samples included nutrients (NO_3^- and PO_4^{3-}), dissolved oxygen (DO), Chl *a*, DIC and TA. The data, collected from USCGC Healy in spring, from RV Xuelong in summer, and from RV Mirai in fall, have been archived in publicly accessible data centers (Table 1).

In the spring cruise, nutrients, DO and Chl *a* were measured onboard. Nutrient samples were determined using a Seal Analytical continuous-flow AutoAnalyzer 3 following a modified procedure after Armstrong et al. (1967). DO was measured using a spectrophotometer following the standard Winkler titration method, with a precision of $\pm 1 \mu\text{mol kg}^{-1}$. Chl *a* measurements were made using a Turner 10-AU fluorometer (Turner Designs, Inc.) (Holm-Hansen et al., 1965) and were calibrated against a pure Chl *a* standard (Sigma). See more description of sampling and analysis of nutrients, DO, and Chl *a* in Arrigo et al. (2017). DIC and TA samples were collected into 250 mL borosilicate glass bottles poisoned with 100 μL saturated HgCl_2 solution to prevent biological activity following the procedure described in Dickson et al. (2007). DIC and TA samples were analyzed at the University of Southampton, UK via coulometric (DIC) and potentiometric (TA) titration methods using a VINDTA 3C (Marianda), with a precision of $\pm 2 \mu\text{mol kg}^{-1}$.

In the summer cruise, nutrient data were measured onboard using a San⁺⁺ automated continuous flow auto-analyzer with a precision of $\pm 2\%$ (SKALAR Inc., Netherlands). The detection limits were 0.1 μM for NO_3^- and 0.03 μM for PO_4^{3-} . Chl *a* samples were measured following similar procedures to the spring expedition. DO was measured onboard using the spectrophotometric method based on Winkler titration with a precision of $\pm 1 \mu\text{mol kg}^{-1}$. See more descriptions of sampling and analysis of nutrients and Chl *a* samples in Zhuang et al. (2020). DIC and TA samples were collected following similar procedures described above, and then were analyzed at the University of Delaware, USA. DIC samples were analyzed using a LiCOR LI 7000 infrared CO_2 detector coupled to an automated DIC analyzer (Apollo SciTech, USA). TA samples were measured via open-cell potentiometric titration system (Apollo SciTech, USA). The precision of the DIC and TA measurements was $\sim 0.1\%$ ($\sim \pm 2 \mu\text{mol kg}^{-1}$; Chen et al., 2015).

In the fall cruise, nutrients were analyzed using QuAAtro system. DO was measured via the spectrophotometric Winkler titration method (Kimoto Electric Co. LTD) following the World Ocean Circulation Experiment Hydrographic Program method (Dickson, 1996). The precision of DO measurement was 0.23 $\mu\text{mol kg}^{-1}$ (Kimoto Electric Co. LTD). Chl *a* was measured using a fluorophotometer (Turner Designs) (Welschmeyer, 1994). Nutrient samples were analyzed following the GO-SHIP Repeat Hydrography Manual (Hydes et al., 2010) using reference materials for nutrients in seawater (Sato et al., 2010). The precision was 0.08% for NO_3^- and 0.14% for PO_4^{3-} . See more descriptions of sampling and analysis of nutrient, DO, and Chl *a* in Nishino et al. (2020). DIC was measured using an automated coulometric analyzer (Nippon ANS, Inc.) with a precision of $\pm 0.7 \mu\text{mol kg}^{-1}$ and TA samples were measured using a custom spectrophotometric system (Nippon ANS, Inc.) with a precision of $\pm 0.57 \mu\text{mol kg}^{-1}$. Note that DIC and TA samples collected in all three cruises were calibrated using certified reference materials (CRMs) from Scripps Institution of Oceanography.

In addition, discrete $p\text{CO}_2$ was calculated with surface TA and DIC (<10 m) to increase the data coverage over temporal and spatial scales. The $p\text{CO}_2$ was calculated by the seacarb package in R (Gattuso et al., 2018) with carbonate dissociation constants of Millero et al. (2006), as recommended by Evans et al. (2015). The uncertainty of $p\text{CO}_2$ values computed from TA and DIC is estimated to be $\pm 18 \mu\text{atm}$ (RMSE) with a mean systematic difference from the observed $p\text{CO}_2$ of 0.5 μatm ($N = 111$).

2.4. Decomposition of Seasonal $p\text{CO}_2$ Change

To explore the dominant drivers for seasonal $p\text{CO}_2$ change in each water mass, we decomposed the net change of $p\text{CO}_2$ into thermal and non-thermal effects, assuming that these two effects altered $p\text{CO}_2$ within a time frame much shorter than the residence time of the water mass on the Chukchi shelf. Therefore, the net change in $p\text{CO}_2$

($\Delta(p\text{CO}_2)$) could be calculated as the difference between the initial $p\text{CO}_2$ ($p\text{CO}_{2\text{ini}}$) under the ice in spring ($538 \pm 68 \mu\text{atm}$) and the observed $p\text{CO}_2$ ($p\text{CO}_{2\text{ob}}$) at a given sampling time:

$$\Delta(p\text{CO}_2) = p\text{CO}_{2\text{ob}} - p\text{CO}_{2\text{ini}} \quad (1)$$

The potential thermal effect on $p\text{CO}_2$ change ($\Delta(p\text{CO}_2)_T$) was driven by the seasonal variation in SST and was quantified by adjusting the initial $p\text{CO}_2$ to the observed temperature (Takahashi et al., 1993):

$$\Delta(p\text{CO}_2)_T = p\text{CO}_{2\text{ini}} \times \exp(0.0423 \times (T_{\text{obs}} - T_{\text{spring}})) - p\text{CO}_{2\text{ini}} \quad (2)$$

where T_{obs} is the observed temperature and T_{spring} is the mean temperature observed under the ice in spring (-1.60°C). The non-thermal effect on $p\text{CO}_2$ change ($\Delta(p\text{CO}_2)_{\text{nT}}$) was mainly driven by the seasonal biological CO_2 drawdown and ice melt, and was calculated as the difference between the observed total net seasonal change and the thermal effect:

$$\Delta(p\text{CO}_2)_{\text{nT}} = \Delta(p\text{CO}_2) - \Delta(p\text{CO}_2)_T \quad (3)$$

2.5. Seasonal CO_2 Flux Calculation

To avoid calculational bias induced by the overweighted impact of highly dense data point concentrated within a small area, we averaged the data points into daily-grids of 0.25° latitude \times 0.25° longitude, and then we calculated seasonal air-sea CO_2 flux for each grid following:

$$\text{FCO}_2 = K_s \cdot k_{\text{CO}_2} \cdot \Delta p\text{CO}_2 \quad (4)$$

where K_s is the solubility of CO_2 and k_{CO_2} is the CO_2 gas transfer velocity. K_s was calculated using underway SST and SSS (Weiss, 1974). The value of k_{CO_2} (cm/hr) is estimated from the second moment of wind speed at 10 m above the sea surface, $\langle U_{10}^2 \rangle$ (Wanninkhof, 2014):

$$k_{\text{CO}_2} = 0.251 \cdot \langle U_{10}^2 \rangle \cdot (\text{Sc}/660)^{-0.5} \cdot \left(1 - \frac{\text{ice}\%}{100}\right) \quad (5)$$

To calculate $\langle U_{10}^2 \rangle$, we used the wind product from the NCEP-DOE Reanalysis 2 data set (<https://www.esrl.noaa.gov/psd/data/gridded/data.ncep.reanalysis2.html>). A regional mean of $\langle U_{10}^2 \rangle$ over the study period was derived from the 6-hr wind speed squared. The term ice% is the sea ice concentration, which is averaged from daily ice% data obtained from the Scanning Multichannel Microwave Radiometer (SMMR) on the Nimbus-7 satellite and the Special Sensor Microwave/Imager (SSM/I) sensors on the Defense Meteorological Satellite Program's (DMSP)-F8, -F11, and -F13 satellites (<https://nsidc.org/data/nsidc-0079>; Comiso, 2017). For the area with heavy ice covered, we adopted Takahashi et al. (2009) approach that for sea ice where satellite observation is $>90\%$ ice cover, a 10% open water area is assumed. In this way, 10% of the open water persisted for CO_2 flux in the area with $>90\%$ ice cover where satellite data with resolution of $25 \text{ km} \times 25 \text{ km}$ fails to resolve fine scale structure, such as leads.

The air-sea CO_2 gradient ($\Delta p\text{CO}_2$) is calculated as:

$$\Delta p\text{CO}_2 = p\text{CO}_2^{\text{sea}} - p\text{CO}_2^{\text{air}} \quad (6)$$

where the $p\text{CO}_2^{\text{sea}}$ is from underway observations and the $p\text{CO}_2^{\text{air}}$ is derived from monthly average atmospheric CO_2 concentrations in dry air ($x\text{CO}_2$ (ppm)) measured at Point Barrow, Alaska (https://www.esrl.noaa.gov/gmd/dv/data/index.php?parameter_name=Carbon%2BDioxide%26frequency=Monthly%2BAverages%26site=BRW; Thoning et al., 2021). Then $x\text{CO}_2$ is corrected for water vapor pressure content to $p\text{CO}_2^{\text{air}}$:

$$p\text{CO}_2^{\text{air}} = x\text{CO}_2 \cdot (\text{Psl} - \text{Pw}) \quad (7)$$

where Psl is sea level pressure and Pw is water vapor pressure. Regional mean Psl over the study period was averaged from a satellite reanalysis product (NCEP-DOE Reanalysis 2, <https://www.esrl.noaa.gov/psd/data/gridded/data.ncep.reanalysis2.html>). Pw was calculated from Psl and SST (Buck, 1981).

2.6. Estimates of Net Community Production

The NCP can be estimated from the nutrient and DIC changes in the upper mixed layer. Since the residence time of water masses on the Chukchi Sea shelf (3–7.5 months) (Stabeno et al., 2018; Woodgate & Peralta-Ferriz, 2021) is longer than the timespan of a phytoplankton bloom (<1–2 months), we can assume that water masses move as a single parcel over the shelf, where physical (mostly warming and freshening) and biogeochemical changes occur over time. Therefore, at any particular location, the observed drawdown of nutrients and DIC in the surface mixed layer can be attributed to NCP. However, nutrient and DIC concentrations are not only influenced by NCP, but also by meltwater/river-runoff dilution, and in the case of DIC, by air-sea CO₂ exchange and CaCO₃ dissolution and formation. Thus, to quantify the biological-induced changes in nutrients, DIC, and TA, we normalized all nutrient (NO₃⁻ and PO₄³⁻), DIC and TA concentrations to a reference salinity (S₀, i.e., mean salinity under the ice in spring) to remove the impact of Arctic Ocean freshwater input into the Pacific winter water. As river discharge impact in spring and early summer is either limited to the estuarine and nearshore areas within the Arctic or treated as part of the Pacific water endmember (Text S1 and Figure S1 in Supporting Information S1), the salinity change in Chukchi Sea is mainly attributed to ice melt dilution for period of interest (spring to early summer); thus, non-zero meltwater endmembers are used (Friis et al., 2003; Jiang et al., 2008):

$$nDIC = \frac{DIC - DIC_{S=0}}{S} \times S_0 + DIC_{S=0} \quad (8)$$

$$nTA = \frac{TA - TA_{S=0}}{S} \times S_0 + TA_{S=0} \quad (9)$$

$$nNO_3^- = \frac{NO_3^- - NO_{3\ S=0}^-}{S} \times S_0 + NO_{3\ S=0}^- \quad (10)$$

The meltwater salinity, DIC and TA values are set as 5, 400 μmol kg⁻¹, 460 μmol kg⁻¹ (Rysgaard et al., 2007), respectively, which are equivalent to DIC_{S=0} = 60 μmol kg⁻¹ and TA_{S=0} = 106 μmol kg⁻¹ (Cai et al., 2010; Ouyang et al., 2020). The contributions of meltwater to NO₃⁻ (μM) and PO₄³⁻ (μM) concentrations are negligible (Clark et al., 2020).

The deficit of nNO₃⁻ (or nPO₄³⁻) is the result of phytoplankton uptake between the time before the phytoplankton bloom begins (t₁) in spring and the time of sampling (t₂). Then, the vertical integral of the deficit of nNO₃⁻ (or nPO₄³⁻) within surface mixed layer is assumed to be equal to NCP at any given location over the time interval between t₁ and t₂ (Δt),

$$NCP_{N\text{-based}} = (nNO_{3\ t_1}^- - nNO_{3\ t_2}^-) MLD / \Delta t \quad (11)$$

Analogue equations of Equations 10 and 11 can be written for nPO₄³⁻. The average mixed layer depth (MLD) of 25 m was used in this study. While this is a highly simplified treatment, the MLD uncertainty would apply equally to C-, N-, and P-based NCP. The estimates of nutrient-based NCP were then converted to carbon units by multiplying by a M C:N:P uptake ratio of 106:16:1 (Arrigo et al., 2017; Codispoti et al., 2013; Hansell et al., 1993; Redfield, 1958).

The nDIC change reflects the influence of both phytoplankton uptake, air-sea CO₂ exchange, and CaCO₃ dissolution and formation. Therefore, we calculated biological-induced nDIC change by subtracting the DIC added by the CO₂ influx and possible CaCO₃ formation and dissolution (CaCO₃ + H₂O + CO₂ ↔ Ca²⁺ + 2HCO₃⁻):

$$NCP_{DIC\text{-based}} = (nDIC_{t_1} \times \rho_{t_1} - nDIC_{t_2} \times \rho_{t_2} - \Delta DIC_{CaCO_3}) \times MLD / \Delta t - CO_2 \text{ flux} \quad (12)$$

where ρ is the water density and CO₂ flux term was calculated following Equation 4. The term of ΔDIC_{CaCO₃} can be quantified as half of the change in salinity-normalized TA (nTA) corrected for the removal of NO₃⁻ to form organic matter (Brewer & Goldman, 1976; Lee, 2001):

$$\Delta DIC_{CaCO_3} = (\Delta nTA \times \rho - \Delta NO_3^-) \times 0.5 \quad (13)$$

Note that due to lack of information we are not able to differentiate biological calcification and the dissolution of CaCO₃ mineral (ikaite) trapped in the melting ice.

2.7. Box Model

The goal of the box model is to investigate how a flexible C:N uptake ratio by phytoplankton affects DIC fixation and air-sea CO₂ fluxes in the Chukchi Sea. Similar box model approaches have been described in previous studies (Ouyang et al., 2020, 2021). Briefly, the initial TA and DIC values were set to the mean value of observations in the surface mixed layer in late spring, and the initial sea surface pCO₂ was calculated from the initial TA and DIC using the seacarb package in R (Gattuso et al., 2018). TA in the subsequent season was linearly interpolated based on observations. For each simulation step, sea surface pCO₂ was calculated from TA and DIC at the corresponding step. The change in DIC inventory (ΔDIC) in the surface mixed layer was calculated as

$$\Delta\text{DIC}_t = (\text{FCO}_{2t} + \text{NCP}_t) \times \tau / (\text{MLD} \times \rho) + \Delta\text{DIC}_{(\text{diluted})t} \quad (14)$$

where FCO_{2t}, NCP_t, and ΔDIC_{(diluted)t} indicate the changes in DIC inventory in the mixed layer induced by the CO₂ air-sea flux, NCP, and dilution by meltwater at simulation time step *t*, respectively. In this case, the simulation time interval (τ) is 1 day. The surface seawater density, ρ , was calculated using SST and SSS. The FCO₂ term was calculated with Equation 4. The ΔDIC_{(diluted)t} term was computed by simplifying the ice melt dilution and assuming that the ratio of TA/DIC in the thin first-year ice nearly equals that in the surface seawater (Rysgaard et al., 2007). Thus,

$$\Delta\text{DIC}_{(\text{diluted})t} = (\text{TA}_{t+1} - \text{TA}_t) / \text{TA}_t \times \text{DIC}_t \quad (15)$$

Because the Chukchi Sea is N-limited during the growing season (Mills et al., 2015, 2018), NCP_t was calculated based on nitrate; NCP_{N-based}. Two scenarios with different C:N uptake ratios were examined in the box model. For the fixed-stoichiometry scenario, a C:N uptake ratio of 6.6 (Redfield ratio) was used. For the non-Redfield scenario, much higher C:N uptake ratios were used (i.e., 10.9 and 12.1 in Table 5). Therefore,

$$\text{NCP}_t = \text{NCP}_{\text{N-based}} \times \text{C:N ratio} \quad (16)$$

And DIC at time step *t* + 1 was iteratively calculated as follows:

$$\text{DIC}_{t+1} = \text{DIC}_t + \Delta\text{DIC}_t \quad (17)$$

With the new DIC and TA, a new pCO₂ was calculated for the next simulation step, and this simulation process repeated until the last day of the simulation.

3. Results

3.1. Sea Surface Temperature, Salinity, and pCO₂

Underway SST, SSS, and pCO₂ were measured during five cruises in the Chukchi Sea, from May through September in 2014, providing a consistent way to examine the seasonal transition of the ocean from a CO₂ source to a sink and to explore the role of changing water masses.

Because sea ice melt began in the southern portion of the Chukchi Sea in early June, we divided the spring observations into two periods: early spring (15–31 May) and late spring (1–21 June 1). Clearly, SST distribution was greatly affected by sea ice (Figure 2a). SST was near freezing ($-1.67 \pm 0.07^\circ\text{C}$) under the ice in the north, while SST in the south was slightly warmer ($-1.28 \pm 0.28^\circ\text{C}$). The location of SST fronts corresponded well with the edge of heavy ice cover around 69.5°N (ice concentration ~80%). However, the distribution of SSS was not as closely correlated with ice as SST was (Figure 2b). In the southern portion of Chukchi Sea, the surface water was relatively fresher due to mixing with newly melted water and river discharge. The saltier water appeared in the eastern and central Chukchi Sea under the ice. Interestingly, relatively warmer and fresher water was also found in the northeast part of Chukchi Sea toward the shelfbreak (Figures 2a and 2b), which was likely due to local ice melt events. The average pCO₂ in the south was $309 \pm 50 \mu\text{atm}$, which was much lower than that in the north ($536 \pm 74 \mu\text{atm}$). Such a contrasting pattern in pCO₂ indicated that the southern ice-free Chukchi Sea had already become a CO₂ sink while the northern ice-covered Chukchi Sea still remained supersaturated with respect to atmospheric CO₂ (~400 μatm) and was a potentially strong CO₂ source in early spring (Figure 2c).

As sea ice retreated northwards in the late spring (Figures 2d–2f), more warm and fresh waters advected from south to north. However, their impacts were confined by sea ice. The SST, SSS, and pCO₂ values in the ice-covered

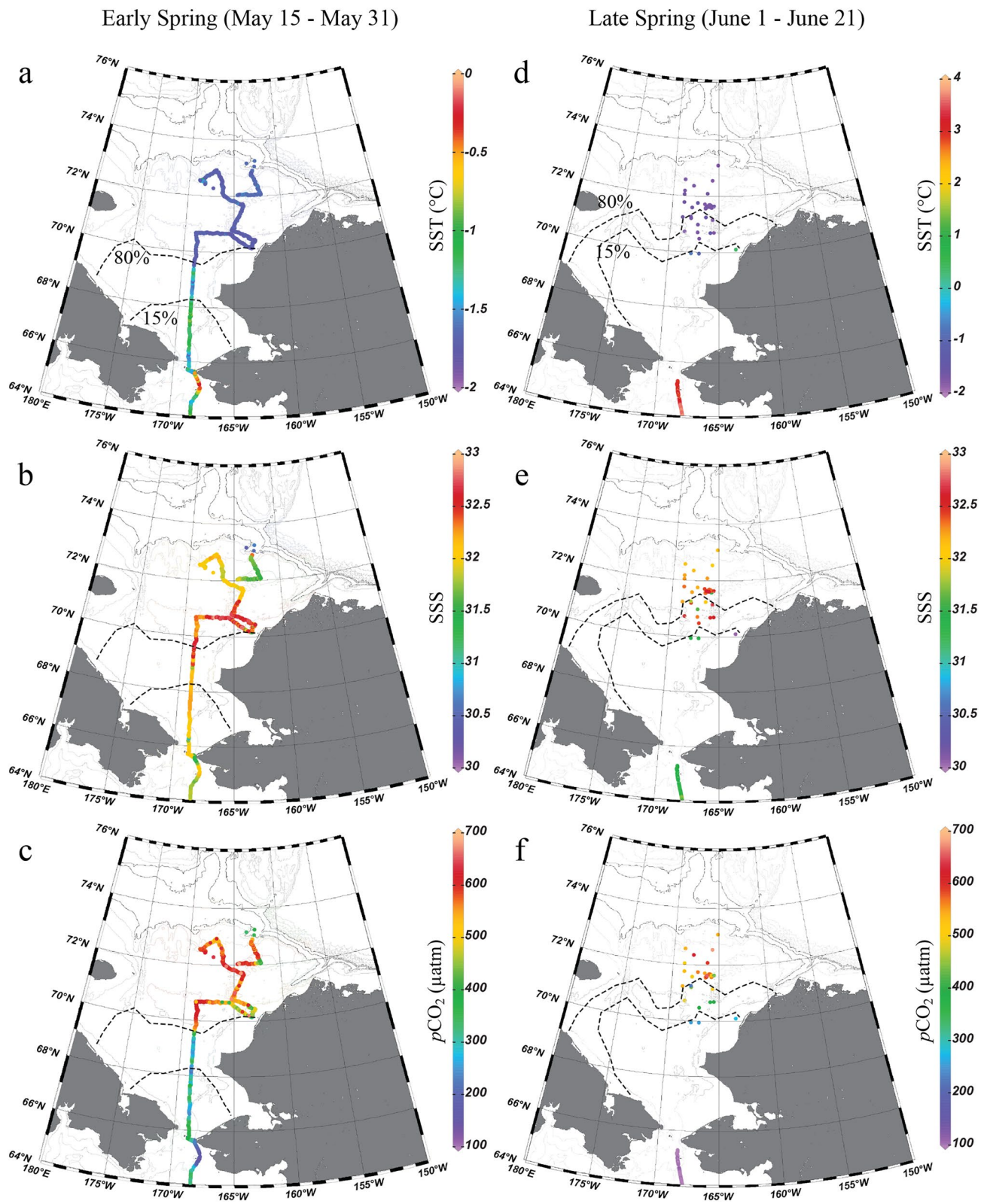


Figure 2. Sea surface temperature, salinity, and $p\text{CO}_2$ in the spring of 2014 in the Chukchi Sea. The observations are presented in two periods, the early spring (15–31 May) and the late spring (1–21 June). The dashed lines indicate the sea ice concentration contours of 15% and 80% on the last day of each period, 31 May (a–c) and 21 June (d–f), showing the possible maximum ice retreat for each period (National Snow and Ice Data Center, Fetterer et al., 2017, <https://doi.org/10.7265/N5K072F8>). Figures were created using Ocean Data View (Schlitzer, 2016).

area were similar to those earlier in the spring. Only a few observations south of the ice edge showed signals of warmer and fresher Pacific summer waters. Although there were no observations in the southern Chukchi Sea during this period, we expect that water there might have become warmer and fresher with much lower $p\text{CO}_2$ compared to early spring, which was confirmed by observations on the last day (21 June) of the spring cruise in the south of Bering Strait (Figures 2d–2f).

In early summer (9 July–7 August), the ice edge retreated further northwards to around 71–72°N (Figures 3a–3f). The mean SST increased to $6.64 \pm 1.22^\circ\text{C}$ in the southern and central Chukchi Sea but remained low ($-0.83 \pm 1.31^\circ\text{C}$) under the ice in the northern Chukchi Sea (Figures 3a and 3d). The distribution of SSS was not only affected by the northward advection of water but also by dilution by meltwater. Compared to spring, the mean SSS (31.0 ± 0.7) over much of the southern and central Chukchi Sea had decreased by 0.5–1.0, although this decrease was more substantial (by 3–4) near the shelfbreak (Figures 3b and 3e). The most notable change in the carbonate system between spring and early summer was a widespread reduction in sea surface $p\text{CO}_2$. The lowest $p\text{CO}_2$ values were found in the vicinity of the Bering Strait in the south and along the ice edge in the northern Chukchi Sea (Figures 3c and 3f).

The Chukchi Sea had become a completely ice-free region in late summer (12 August–9 September 9; Figures 3g–3l). SST continued to increase over the entire Chukchi shelf (Figures 3g and 3j). The highest SST appeared in the middle of August along the Alaska coast, reaching up to $\sim 11^\circ\text{C}$ (Figure 3g). The SSS showed a similar distribution as in early summer, with saltier water in the southern and central Chukchi Sea and fresher water in the eastern and northern portion as a result of massive sea-ice melt and river discharge (Figures 3h and 3k). Compared to early summer, the mean sea surface $p\text{CO}_2$ in late summer increased from $202 \pm 63 \mu\text{atm}$ to $265 \pm 69 \mu\text{atm}$ but remained much lower than the atmospheric $p\text{CO}_2$ (Figures 3i and 3l). It is noteworthy that the lowest $p\text{CO}_2$ was observed repeatedly north of Bering Strait and in the area surrounding Hanna Shoal (Figures 3i and 3l).

Between late summer and fall, the mean SST over the entire shelf decreased from $5.42 \pm 3.04^\circ\text{C}$ to $3.49 \pm 1.73^\circ\text{C}$, while the mean SSS remained nearly unchanged (Figures 4a and 4b). For most of the Chukchi Sea, surface water $p\text{CO}_2$ was lower than the atmospheric $p\text{CO}_2$, averaging $283 \pm 50 \mu\text{atm}$, indicating that the CO_2 sink lasted into fall. However, extremely high $p\text{CO}_2$ started to appear in the northern Bering Sea along the western pathway of Pacific Summer Water (Figure 4c).

3.2. Water Column Structure

Discrete samples of biogeochemical parameters were collected during three cruises (Table 1). Since these three cruises conducted survey sections along the Central Channel, we are able to show the seasonal evolution of biogeochemical properties in the water column along a transect from the Bering Strait extending to the shelf break in the northern Chukchi Sea.

In early spring, water columns on the Chukchi shelf were well mixed, exhibiting little vertical structure for most biogeochemical properties (Figure 5). The exceptions were a subsurface (20–30 m) Chl *a* maximum in the southern Chukchi Sea (Figure 5g) and the frontal structures of large gradient in DIC and NO_3^- across the shelf breaks (73°N; Figures 5f and 5h). However, latitudinal patterns were significantly different from the south to the north, which was due to different levels of primary production regulated by the timing of ice melting. Seawater temperature and salinity under the ice were within a narrow range of -1.78°C to -1.60°C and 32 to 33, respectively, indicating that during this period, almost all waters on the northern shelf were NVWW (Figure 5d). Low concentrations of Chl *a* ($< 1 \mu\text{g l}^{-1}$), high NO_3^- ($> 15 \mu\text{M}$), and positive apparent oxygen utilization (AOU) beneath the ice suggested that the spring bloom had not yet started there (Figures 5g–5i) and the ambient high DIC was likely accumulated from remineralization in the previous winter water (Figure 5f). In contrast, primary production within RWW had begun in the southern Chukchi Sea, indicated by a much higher Chl *a* concentration ($> 4 \mu\text{g l}^{-1}$), lower NO_3^- , and negative AOU (Figures 5g–5i). As a result, mean DIC in the south was $\sim 100 \mu\text{mol kg}^{-1}$ lower than that in the north (Figure 5f and Table 3).

A few weeks later, as the ice conditions changed, the water at the ice edge became warmer and fresher as a result of local sea ice melt freshening together with atmospheric heating (70.5°N; Figures 6a and 6b). Although most water columns still consisted of NVWW and were well mixed, a two-layer structure appeared in the southernmost stations (Figure 6c), indicating that seasonal stratification of the water column had begun. In addition, the Chl *a*

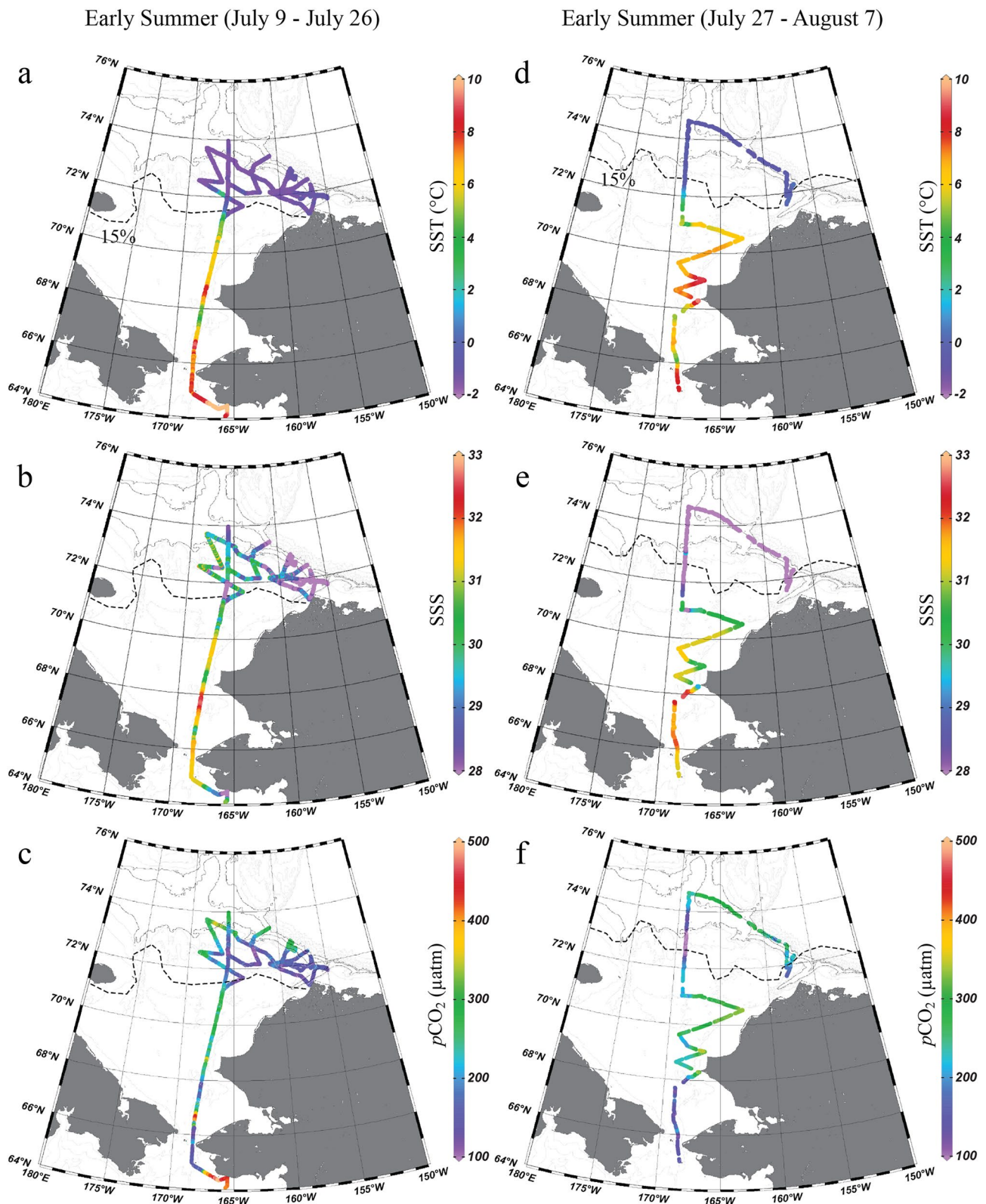


Figure 3. Sea surface temperature, salinity, and $p\text{CO}_2$ in the summer of 2014 in the Chukchi Sea. The observations are presented in four periods depending on the timing of cruises, 9–26 July (a–c), 27 July–7 August (d–f), 12–24 August (g–i) and 3–9 September (j–l). The dashed lines indicate the 15% sea ice concentration contour on the last day of each period, 26 July (a–c), 7 August (d–f), 24 August (g–i) and 9 September (j–l), showing the possible maximum ice retreat for each period (National Snow and Ice Data Center, Fetterer et al., 2017, <https://doi.org/10.7265/N5K072F8>). Figures were created using Ocean Data View (Schlitzer, 2016).

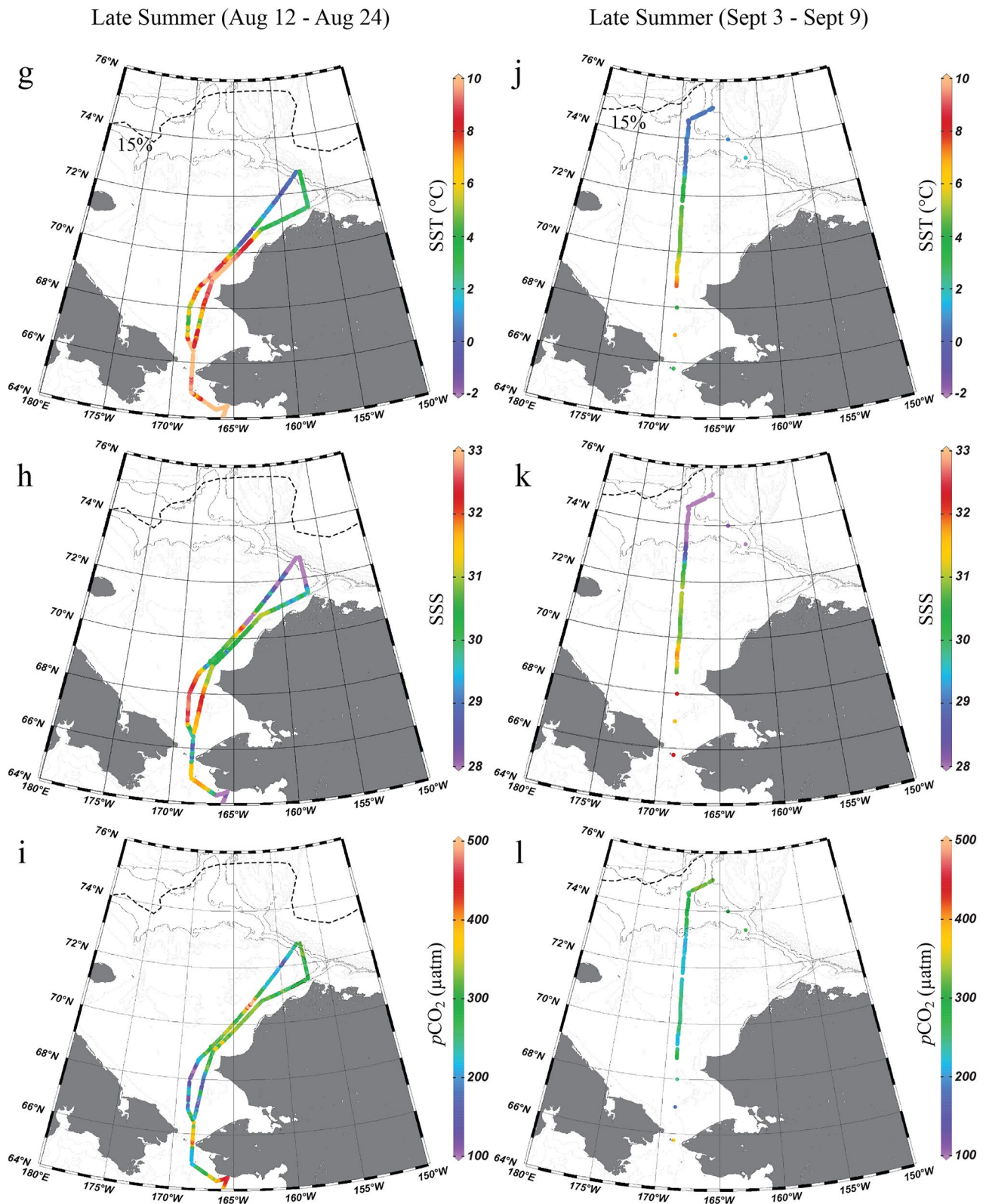


Figure 3. (Continued)

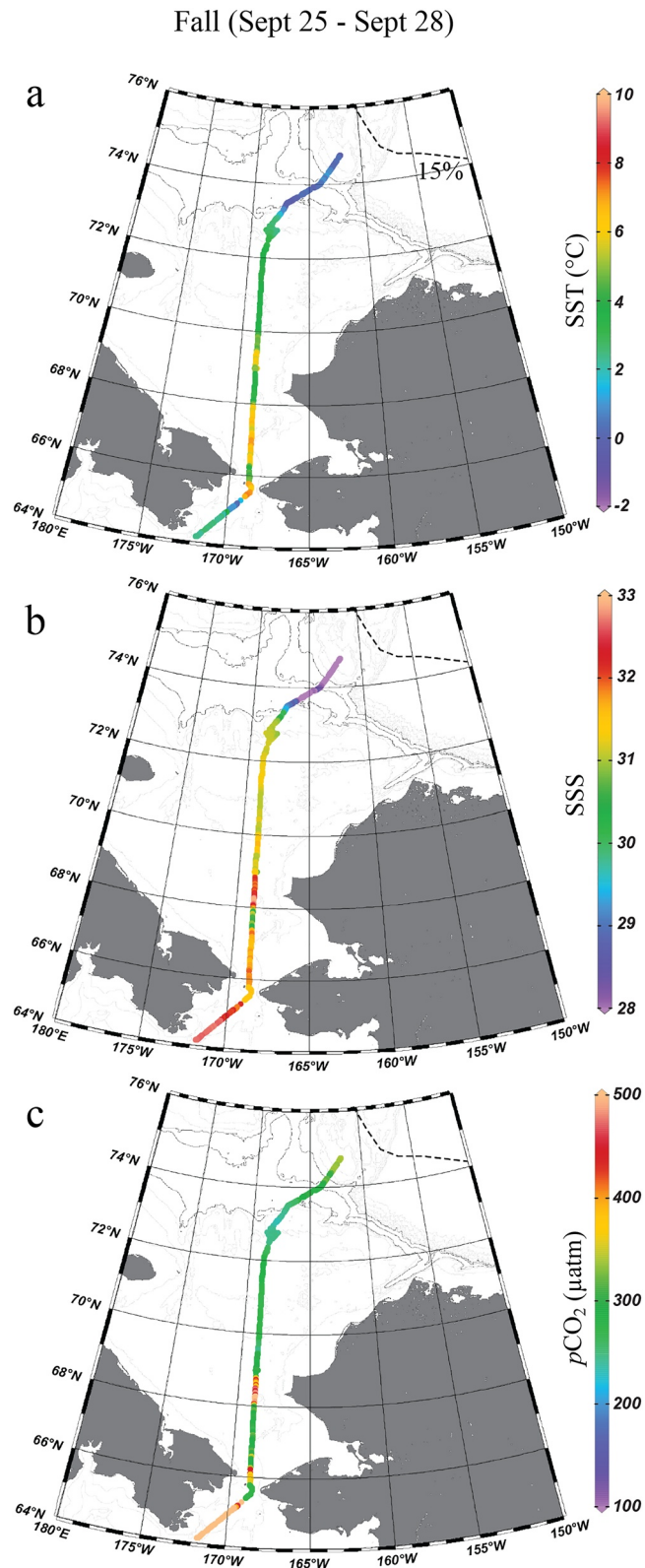


Figure 4. Sea surface temperature, salinity, and $p\text{CO}_2$ in the fall of 2014 (25–28 September) in the Chukchi Sea. The dashed lines indicate the 15% sea ice concentration contour on the last day of survey, 28 September (j–l), showing the possible maximum ice retreat for each period (National Snow and Ice Data Center, Fetterer et al., 2017, <https://doi.org/10.7265/N5K072F8>). Figures were created using Ocean Data View (Schlitzer, 2016).

Table 3
Seasonal Variations in Biogeochemical Properties in the Water Column

Periods	Layers	Temperature (°C)		Salinity		TA ($\mu\text{mol kg}^{-1}$)		DIC ($\mu\text{mol kg}^{-1}$)		AOU ($\mu\text{mol kg}^{-1}$)		Chl <i>a</i> ($\mu\text{g l}^{-1}$)		NO ₃ ⁻ (μM)		PO ₄ ³⁻ (μM)	
		Southern Chukchi	Northern Chukchi	Southern Chukchi	Northern Chukchi	Southern Chukchi	Northern Chukchi	Southern Chukchi	Northern Chukchi	Southern Chukchi	Northern Chukchi	Southern Chukchi	Northern Chukchi	Southern Chukchi	Northern Chukchi	Southern Chukchi	Northern Chukchi
Early spring	Surface	-1.28 ± 0.19	-1.71 ± 0.04	31.9 ± 0.4	32.1 ± 0.6	2,205 ± 7	2,225 ± 28	2,068 ± 35	2,173 ± 41	-13.9 ± 3.5	35.6 ± 23.2	4.4 ± 3.1	0.9 ± 1.7	9.57 ± 5.29	10.54 ± 3.95	1.33 ± 0.30	1.66 ± 0.32
	Bottom	-1.03 ± 0.15	-1.74 ± 0.04	32.2 ± 0.3	32.4 ± 0.4	2,212 ± 28	2,236 ± 18	2,112 ± 70	2,191 ± 27	-27.0 ± 25.8	49.4 ± 20.2	2.4 ± 3.2	0.5 ± 1.2	10.3 ± 3.30	12.18 ± 3.11	1.41 ± 0.27	1.82 ± 0.27
Late spring	Surface	NA	-1.61 ± 0.36	NA	32.2 ± 0.5	NA	2,229 ± 23	NA	2,153 ± 47	NA	14.3 ± 38.0	NA	2.8 ± 2.2	NA	10.57 ± 4.33	NA	1.59 ± 0.35
	Bottom	NA	-1.73 ± 0.04	NA	32.6 ± 0.2	NA	2,243 ± 13	NA	2,188 ± 23	NA	40.9 ± 30.1	NA	2.9 ± 3.1	NA	13.23 ± 2.81	NA	1.89 ± 0.26
Early Summer	Surface	5.95 ± 1.80	3.76 ± 2.79	31.4 ± 1.0	30.7 ± 0.9	2,187 ± 40	2,154 ± 37	1,940 ± 49	1,954 ± 51	-44.6 ± 42.0	-8.2 ± 59.5	1.4 ± 1.2	1.8 ± 3.2	0.27 ± 0.20	0.62 ± 1.51	0.46 ± 0.11	0.62 ± 0.20
	Bottom	3.93 ± 1.61	-0.42 ± 0.99	31.9 ± 0.6	32.1 ± 0.4	2,204 ± 31	2,225 ± 25	2,215 ± 64	2,067 ± 78	4.3 ± 34.6	39.9 ± 54.6	2.6 ± 4.0	2.6 ± 2.4	3.67 ± 4.50	4.96 ± 8.29	0.84 ± 0.34	1.07 ± 0.55
Late Summer	Surface	4.46 ± 1.55	NA	32.1 ± 0.3	NA	2,199 ± 20	NA	2,012 ± 61	NA	-16.6 ± 17.1	NA	18.8 ± 10.0	NA	3.95 ± 3.46	NA	0.75 ± 0.35	NA
	Bottom	2.27 ± 0.27	NA	32.5 ± 0.2	NA	2,211 ± 12	NA	2,161 ± 24	NA	88.5 ± 13.7	NA	2.3 ± 0.7	NA	18.01 ± 2.53	NA	2.08 ± 0.25	NA
Fall	Surface	5.33 ± 0.99	3.10 ± 0.58	31.6 ± 0.2	31.1 ± 0.2	2,180 ± 14	2,249 ± 12	2,008 ± 27	1,971 ± 13	-5.0 ± 4.8	-4.4 ± 11.4	5.8 ± 2.9	0.7 ± 0.4	2.24 ± 1.07	0.06 ± 0.03	0.62 ± 0.12	0.45 ± 0.03
	Bottom	3.15 ± 0.37	0.66 ± 1.56	32.4 ± 0.4	32.2 ± 0.3	2,207 ± 21	2,208 ± 15	2,111 ± 45	2,105 ± 59	44.7 ± 32.0	35.1 ± 48.7	2.2 ± 1.1	0.6 ± 0.3	11.53 ± 4.48	4.60 ± 2.51	1.56 ± 0.35	1.34 ± 0.41

Note. Mean and standard deviation are reported for both the surface mixed layer and the bottom layer. No observations were made in the southern Chukchi Sea in late spring and in northern Chukchi Sea in late summer.

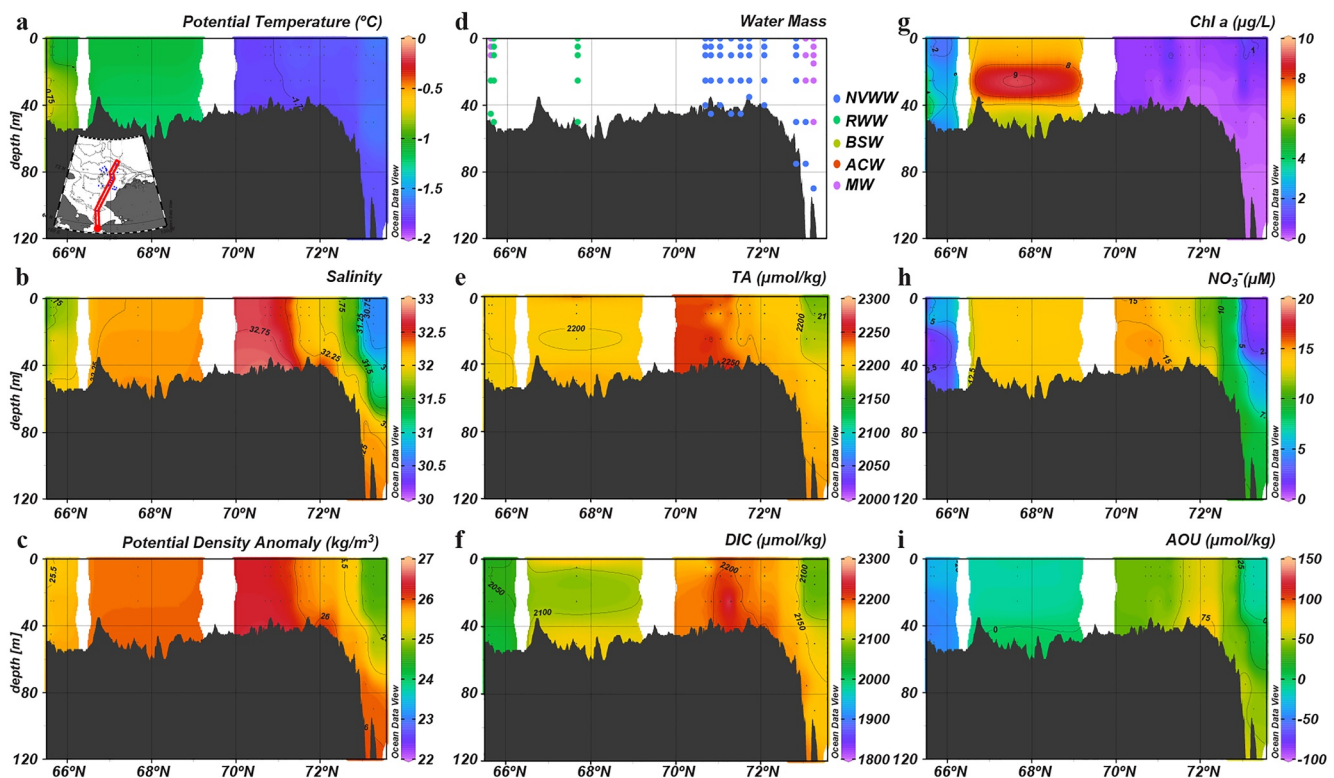


Figure 5. Vertical distributions of physical and biogeochemical parameters in the early spring (15–31 May) along the central Chukchi Sea. (a) Potential temperature, (b) salinity, (c) potential density anomaly, (d) water mass, (e) TA, (f) dissolved inorganic carbon, (g) chlorophyll *a*, (h) NO_3^- and (i) apparent oxygen utilization.

concentration increased to $2.8 \pm 2.2 \mu\text{g l}^{-1}$ and the previously positive AOU had turned negative, indicating net oxygen production by a phytoplankton bloom (Figure 6i). The late-spring ice retreat further strengthened primary production in the northern Chukchi Sea. In turn, the associated biological CO_2 drawdown resulted in lower DIC in the surface layer (Figure 6f).

Conditions during the early summer transect were vastly different from the spring conditions (Figure 7). The fully mixed water column representative of spring conditions had transformed into a clear two-layer structure with a shallow, warm and fresh surface mixed layer with ACW properties separated by a halocline from BSW and winter water near the bottom (Figures 7a and 7d). Strong primary production over the shelf led to a large reduction in DIC and NO_3^- in the surface mixed layer (Figures 7f and 7h; Table 3). Simultaneously, the surface extremely high O_2 ($\text{AOU} < -100 \mu\text{mol kg}^{-1}$) coincided with the subsurface Chl *a* maximum in the north of Bering Strait and over the shelfbreak (Figures 7g and 7i). Interestingly, the surface extremely low NO_3^- ($< 1 \mu\text{M}$) and supersaturated DO extended throughout the water column in the central Chukchi Sea ($68^\circ\text{N} - 70^\circ\text{N}$ Figures 7h and 7i), which were likely induced by local mixing events occasionally breaking the two-layer structure or a mechanical overturning induced by internal wave mixing (Kawaguchi et al., 2015; Nishino et al., 2015).

Although we only have observations in the southern Chukchi Sea and in the Canada Basin (i.e., no data in the central and northern shelf) in late summer, it is likely that the strong two-layer stratification remained in the water column over most of the Chukchi Sea (Figure 8). The highest Chl *a* concentration ($> 25 \mu\text{g l}^{-1}$) repeatedly appeared at the similar location in the north of Bering Strait associated with BSW (68°N ; Figures 8d and 8g) but AOU increased from < -100 to $\sim -30 \mu\text{mol kg}^{-1}$ (Figure 8i). The surface DIC in the southern Chukchi Sea (probably in the northern Chukchi Sea as well) became higher than in early summer by $\sim 100 \mu\text{mol kg}^{-1}$ (Figure 8f). As the water column stratification strengthened, the gradients in DIC, NO_3^- and AOU between surface and bottom layers became larger (Figures 8f, 8h and 8i; Table 3). The highest NO_3^- ($> 20 \mu\text{M}$) was observed in the bottom waters in the southern Chukchi Sea.

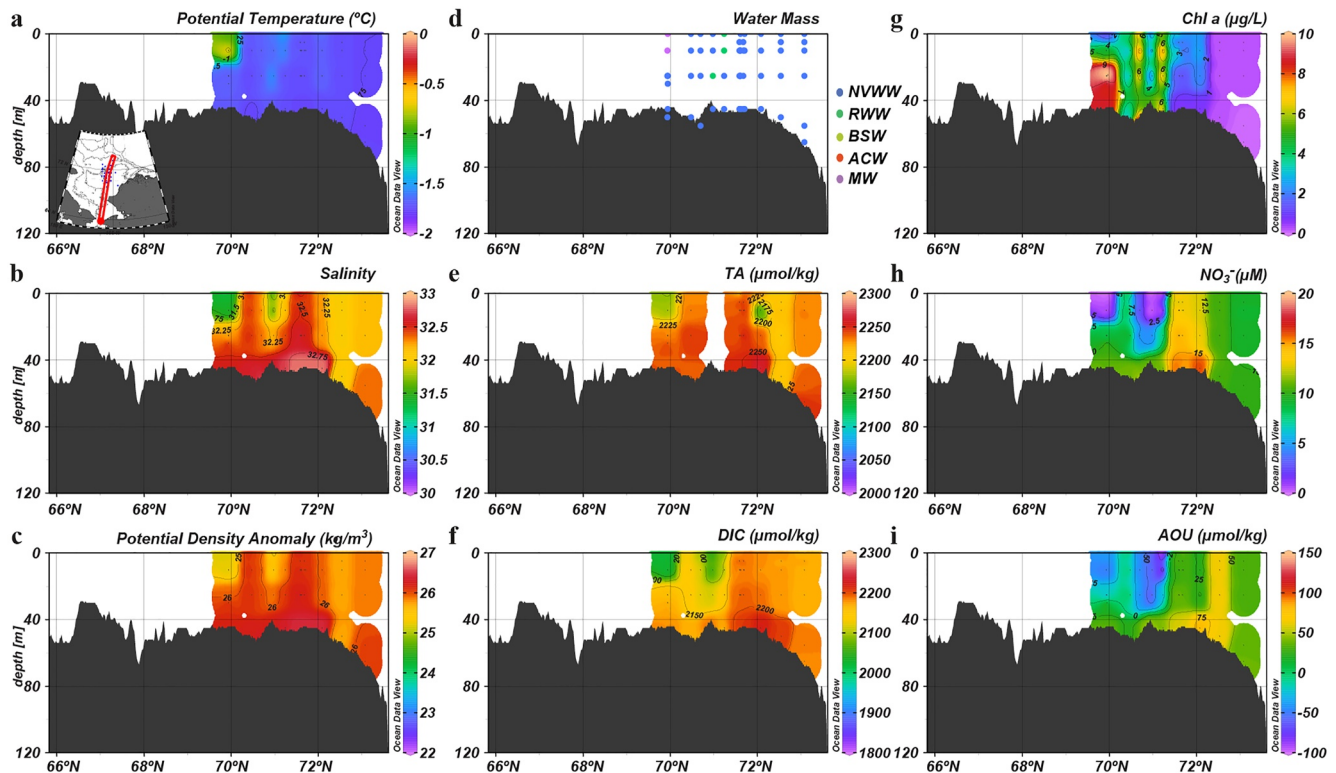


Figure 6. Vertical distributions of physical and biogeochemical parameters in the late spring (1–21 June) along the central Chukchi Sea. (a) Potential temperature, (b) salinity, (c) potential density anomaly, (d) water mass, (e) TA, (f) dissolved inorganic carbon, (g) chlorophyll *a*, (h) NO_3^- and (i) apparent oxygen utilization.

Three weeks later in fall, the stratified vertical structure persisted over most of the shelf area (Figures 9a–9d). However, a widespread reduction in Chl *a* concentrations suggested that primary production had become much weaker. High Chl *a* concentrations were only observed in the biological hot spot in the southern Chukchi Sea (68°N; Figure 9g), which was present throughout the entire growing season. NO_3^- became depleted in the surface waters (Figure 9h), limiting further phytoplankton growth, while replenishment of NO_3^- was observed in bottom waters in the southern Chukchi Sea. Consequently, surface O_2 approached equilibrium with the atmosphere (AOU was $\sim 0 \mu\text{mol kg}^{-1}$) and surface DIC remained the same as it was in late summer (Figures 9f and 9i).

4. Discussion

4.1. Water Mass Evolution and CO_2 Flux

Seasonal evolution of water masses affects primary production and subsequently air-sea CO_2 uptake. To investigate the correlation between water mass change and ocean CO_2 uptake, we first illustrate the relationship between water mass properties and seasonal change in sea surface $p\text{CO}_2$ in T/S diagrams (Figure 10). In spring, most of the net change in $p\text{CO}_2$ was negative since a high $p\text{CO}_2$ value (i.e., 538 μatm) in the earlier winter water under the ice was used as the reference value (Figure 10a). The high $p\text{CO}_2$ values that exceeded atmospheric $p\text{CO}_2$ were concentrated within the cold and salty NVWW and RWW beneath the ice, which was resulted from remineralization in and vertical mixing of waters from the previous winter (Figure 10a). As sea ice started to retreat in late spring and early summer, the dilution by meltwater and strong biological CO_2 uptake led to extremely low ($<100 \mu\text{atm}$) $p\text{CO}_2$ along the ice edge (Figures 3c and 3f) with the largest seasonal reduction in the early-season meltwater (Early-MW; Figure 10b). These two processes primarily triggered the transition from a CO_2 source to a sink within a few weeks. During this period, the average CO_2 flux changed from $1.1 \pm 1.1 \text{ mmol m}^{-2} \text{ d}^{-1}$ (from sea to air, or a source) to $-7.2 \pm 3.4 \text{ mmol m}^{-2} \text{ d}^{-1}$ (from air to sea, or a sink) in the northern Chukchi Sea (Figures 11a and 11b; Table 4). As the season progressed, the surface NVWW and RWW were largely

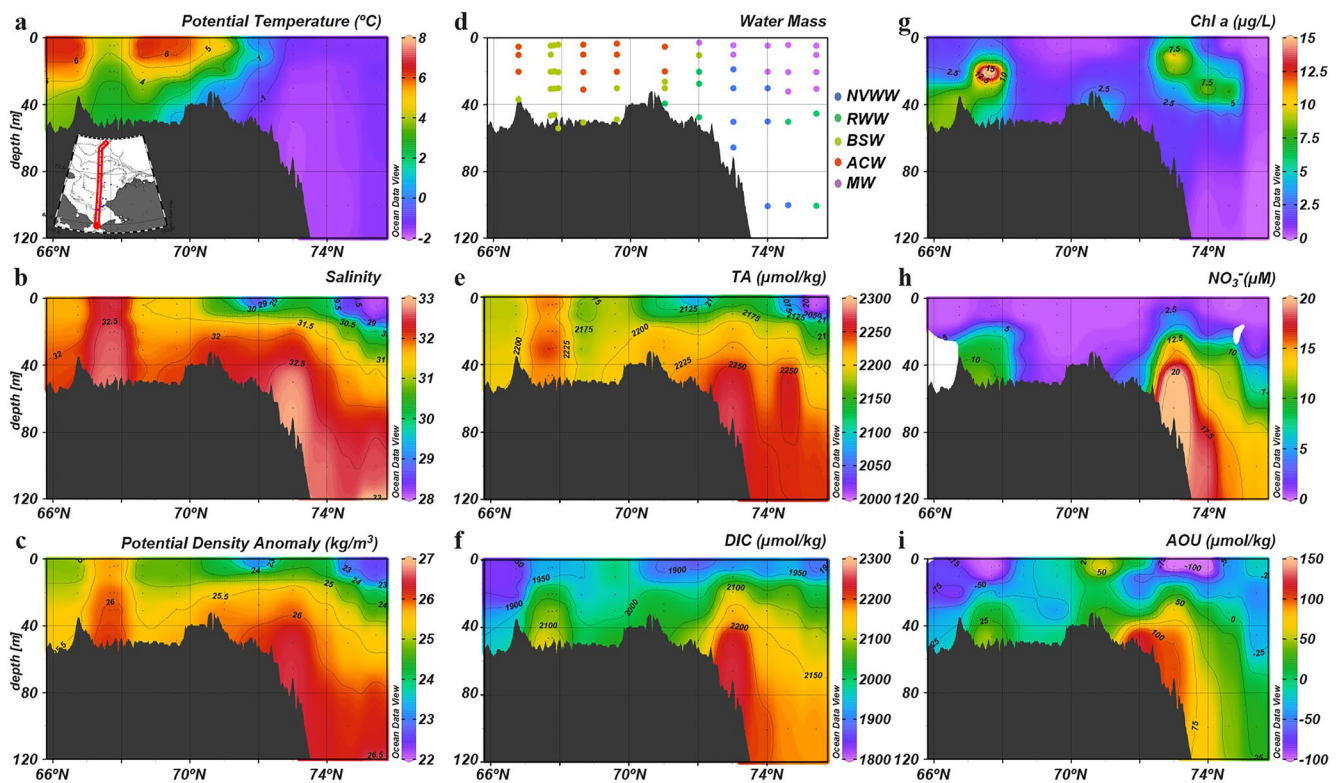


Figure 7. Vertical distributions of physical and biogeochemical parameters in the early summer (27 July–7 August) along the central Chukchi Sea. (a) Potential temperature, (b) salinity, (c) potential density anomaly, (d) water mass, (e) TA, (f) dissolved inorganic carbon, (g) chlorophyll *a*, (h) NO_3^- and (i) apparent oxygen utilization. Note that the color scale of chlorophyll *a* concentration is different from that of Figures 5h, 6h and 9h.

transformed or replaced by summer Pacific waters (i.e., ACW and BSW). Consequently, the nutrient-rich BSW sustained strong primary production and resulted in another extremely strong CO_2 uptake center in the southern Chukchi Sea north of the Bering Strait ($\sim 68^\circ\text{N}$, Figure 11c), whereas the warmer ($\text{SST} > 8^\circ\text{C}$), relatively nutrient-poor ACW had relatively weaker CO_2 uptake along the eastern coastal area (Figure 11c). We noticed a small area of CO_2 efflux in the eastern Chukchi Sea in late summer (Figure 11c) and an area of CO_2 source water in the BSW regime in the southern Chukchi Sea in fall ($\sim 69^\circ\text{N}$; Figure 11d). These high $p\text{CO}_2$ surface waters were likely due to local vertical mixing as energetic currents in this area of shallow depths (< 50 m) could break down stratified vertical structure and bring high $p\text{CO}_2$ bottom water up to the surface (Brown et al., 2015). The regional mean CO_2 flux in late summer and fall were estimated to range from -18.3 ± 8.9 to -10.5 ± 8.4 $\text{mmol m}^{-2} \text{d}^{-1}$ in the southern Chukchi Sea and from -13.3 ± 6.6 to -21.1 ± 2.9 in the northern Chukchi Sea (Table 4).

Decomposition of the seasonal change in $p\text{CO}_2$ provides more insight into the controlling drivers. Between spring and early summer, the largest reduction in $p\text{CO}_2$ was observed in the early-season MW and BSW, while the $p\text{CO}_2$ reduction in the ACW was relatively less (Figure 10b). Specifically, the warm ACW and river runoff have the largest thermal effect on changing $p\text{CO}_2$; a warming of more than 10°C in SST along could potentially increase $p\text{CO}_2$ by ~ 300 μatm (Figure 10f). In contrast, thermal effects were the relatively weaker driver for $p\text{CO}_2$ change in both the BSW and MW (Figure 10f). In addition, the nutrient-rich BSW provided a continued nutrient supply for sustaining primary production and biological CO_2 drawdown along the Central Channel pathway. The strong reduction of $p\text{CO}_2$ within BSW and MW domains (Figure 10j) even exceeded the increase induced by warming (Figure 10f), resulting in a net decrease in $p\text{CO}_2$ and a strong CO_2 sink (Figures 10b and 11b). Similar patterns existed in the following seasons (Figures 10, 11c and 11d).

As the CO_2 uptake mainly occurred within Pacific Summer Water and thermal and non-thermal effects had different impacts on CO_2 flux in different water masses, we estimated CO_2 fluxes separately in two types of water masses: the ACW (including RW) and non-ACW (including BSW and MW but excluding NVWW and RWW). We found that the CO_2 uptake potential in the nutrient-rich non-ACW was significantly larger than that in the

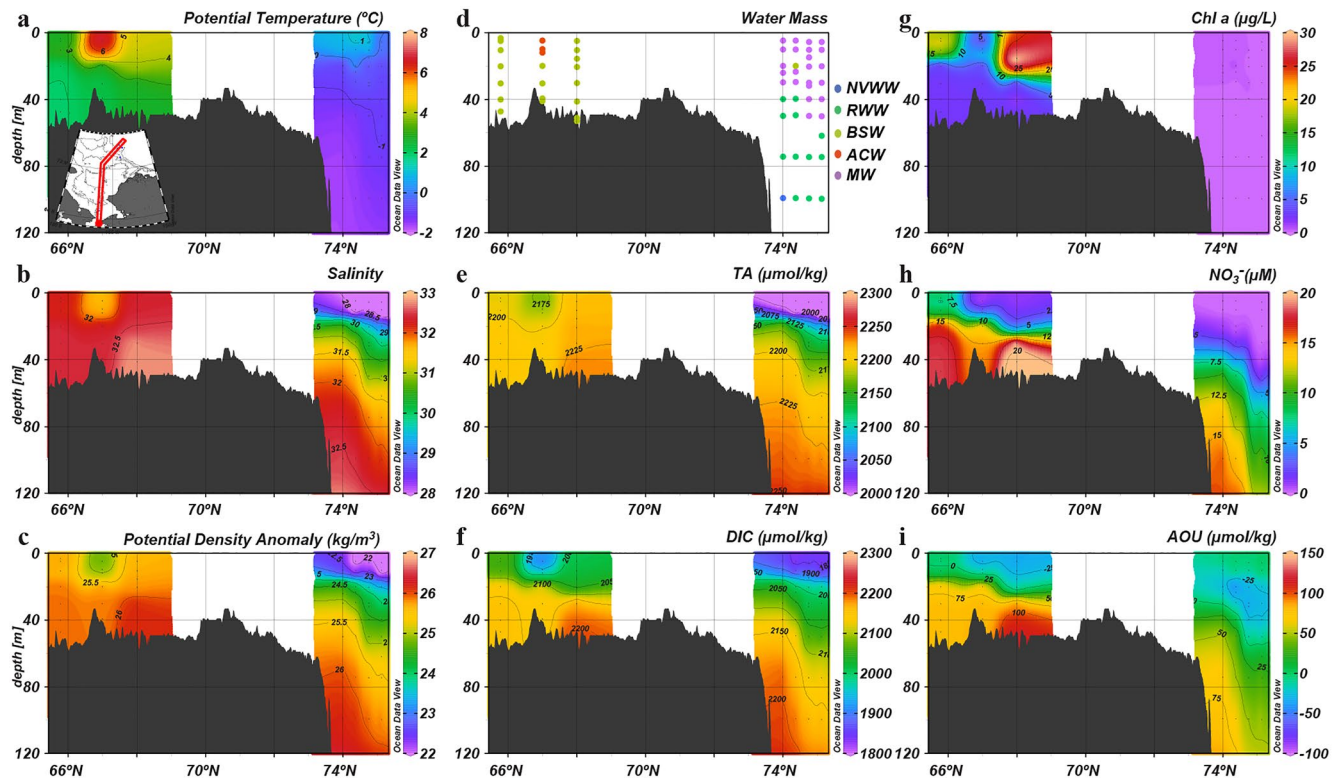


Figure 8. Vertical distributions of physical and biogeochemical parameters in the late summer (3–9 September) along the central Chukchi Sea. (a) Potential temperature, (b) salinity, (c) potential density anomaly, (d) water mass, (e) TA, (f) dissolved inorganic carbon, (g) chlorophyll *a*, (h) NO_3^- and (i) apparent oxygen utilization. Note that the color scale of chlorophyll *a* concentration is different from that of Figures 5h, 6h and 9h.

relatively nutrient-poor ACW in the southern Chukchi Sea during summer months (Table 4). Such difference became less contrasting because these two water masses tended to have more similarities as they were modified by mixing, meltwater input, and other local processes in the northern Chukchi Sea (Table 4). This finding has important implications for CO_2 uptake in the Chukchi Sea. Woodgate (2018) found that annual inflow of Pacific waters has increased by more than 50% from 1990 to 2015, but there was no significant trend in annual mean flow in the ACC. Corlett and Pickart (2017) also confirmed that BSW (non-ACW) increased relative to ACW on the Chukchi slope from 2002 to 2004 to 2009–2014. Thus, non-ACW was likely responsible for the increase in total annual flow. If this is confirmed to be the case, we suggest that the Chukchi Sea will be a greater CO_2 sink in the future, as non-ACW will play a bigger role in CO_2 uptake.

4.2. Water Mass Evolution and Net Community Production

Spatial and temporal variations in water mass distributions substantially affect primary production in the Chukchi Sea during the growing season. In spring, both the southern and northern Chukchi Sea were largely occupied by the winter water (NVWW and RWW), which provided sufficient nutrients for phytoplankton to bloom (Figures 12a–12d; Arrigo et al., 2017). From late spring to early summer, winter waters were gradually transformed to or replaced by the warmer summer waters (BSW and ACW), particularly in the surface layer (Figure 12). At the same time, both normalized nitrate (nNO_3^-), phosphate (nPO_4^{3-}), and DIC (nDIC) decreased rapidly as a result of strong consumption due to phytoplankton growth. In late summer and fall, only a small portion of RWW existed in the bottom layer in the northern Chukchi Sea, while BSW and ACW accounted for the majority of surface water over the entire Chukchi Sea (Figure 12). For the bottom layer, NO_3^- and PO_4^{3-} were replenished by a combination of advection of nutrient-rich BSW and possible vertical mixing from the bottom layer. This input of NO_3^- and PO_4^{3-} exceeded the biological drawdown in the southern Chukchi Sea, which resulted in a net increase in nNO_3^- and nPO_4^{3-} concentrations in both the surface and bottom layers (Figures 12a and 12c).

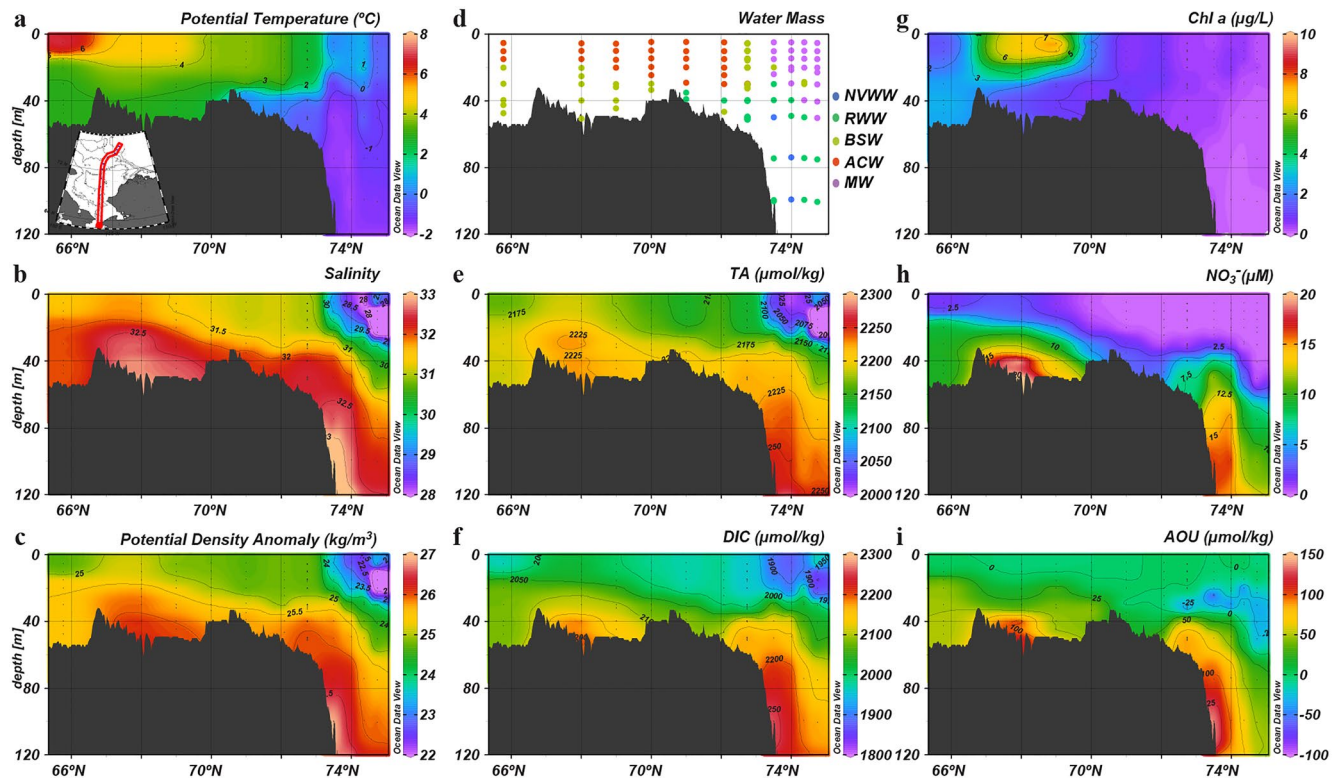


Figure 9. Vertical distributions of physical and biogeochemical parameters in the fall (24–28 September) along the central Chukchi Sea. (a) Potential temperature, (b) salinity, (c) potential density anomaly, (d) water mass, (e) TA, (f) dissolved inorganic carbon, (g) chlorophyll *a*, (h) NO_3^- and (i) apparent oxygen utilization.

However, in the northern Chukchi Sea, nNO_3^- concentration remained depleted and nPO_4^{3-} was the same in the surface layer but both increased in the bottom waters (Figures 12b and 12d). The high residual nNO_3^- and nPO_4^{3-} in the bottom water were likely the remaining within winter waters rather than BSW delivery (Zheng et al., 2021).

As primary production is the main driver modifying water column biogeochemical properties during the growing season, we estimated NCP using the observed drawdown of nutrients (nNO_3^- and nPO_4^{3-}) and nDIC in the surface mixed layer. The spring concentrations of nNO_3^- , nPO_4^{3-} and nDIC were used as an initial condition to determine the subsequent biological drawdown by NCP. As the largest changes were observed in the period between spring and early summer, which were also associated with the most evident water mass evolution, therefore, we will mainly focus on this period in the following discussion.

Although there were no observations in late spring in the southern Chukchi Sea (Figures 12a, 12c and 12e), a water mass analysis showing that the winter water still made up most of the southern Chukchi Sea during this period (Pacini et al., 2019). Based on that, we assume that water parcel in the southern Chukchi Sea between early spring and early summer was not greatly changed and it is still appropriate to estimate NCP based on the deficits of nutrients and nDIC . The decreases of nDIC in the surface mixed layer between spring and early summer were 79 ± 87 and $95 \pm 51 \mu\text{mol kg}^{-1}$, respectively, in the southern and northern Chukchi Sea (Figures 12e and 12f; Table 5). After correcting for air-sea gas exchange and CaCO_3 formation and dissolution, these nDIC deficits yield mean NCP estimates of 38.4 ± 26.2 and $61.4 \pm 20.0 \text{ mmol C m}^{-2} \text{ d}^{-1}$, respectively, in the southern and northern Chukchi Sea (Table 5). Our nDIC -based NCP estimates in 2014 were comparable with NCP estimates made using a similar approach in early summer in 2004 in the northern Chukchi Sea (Mathis et al., 2009). During the same period, nNO_3^- in the surface mixed layer was fully depleted over the entire Chukchi Sea (Figures 12a and 12b). Such NO_3^- depletion was also observed in early summer in 2010 and 2011 (Brown et al., 2015; Lowry et al., 2015). The mean nNO_3^- deficits in 2014 were 10.24 ± 0.20 and $9.92 \pm 1.57 \mu\text{M}$ in the southern and northern Chukchi Sea, respectively (Table 5), giving an NCP of 3.51 ± 0.07 and $5.06 \pm 0.80 \text{ mmol N m}^{-2} \text{ d}^{-1}$ in the southern and northern Chukchi Sea, respectively (Table 5). Because the mean nPO_4^{3-} deficits were 1.19 ± 0.11

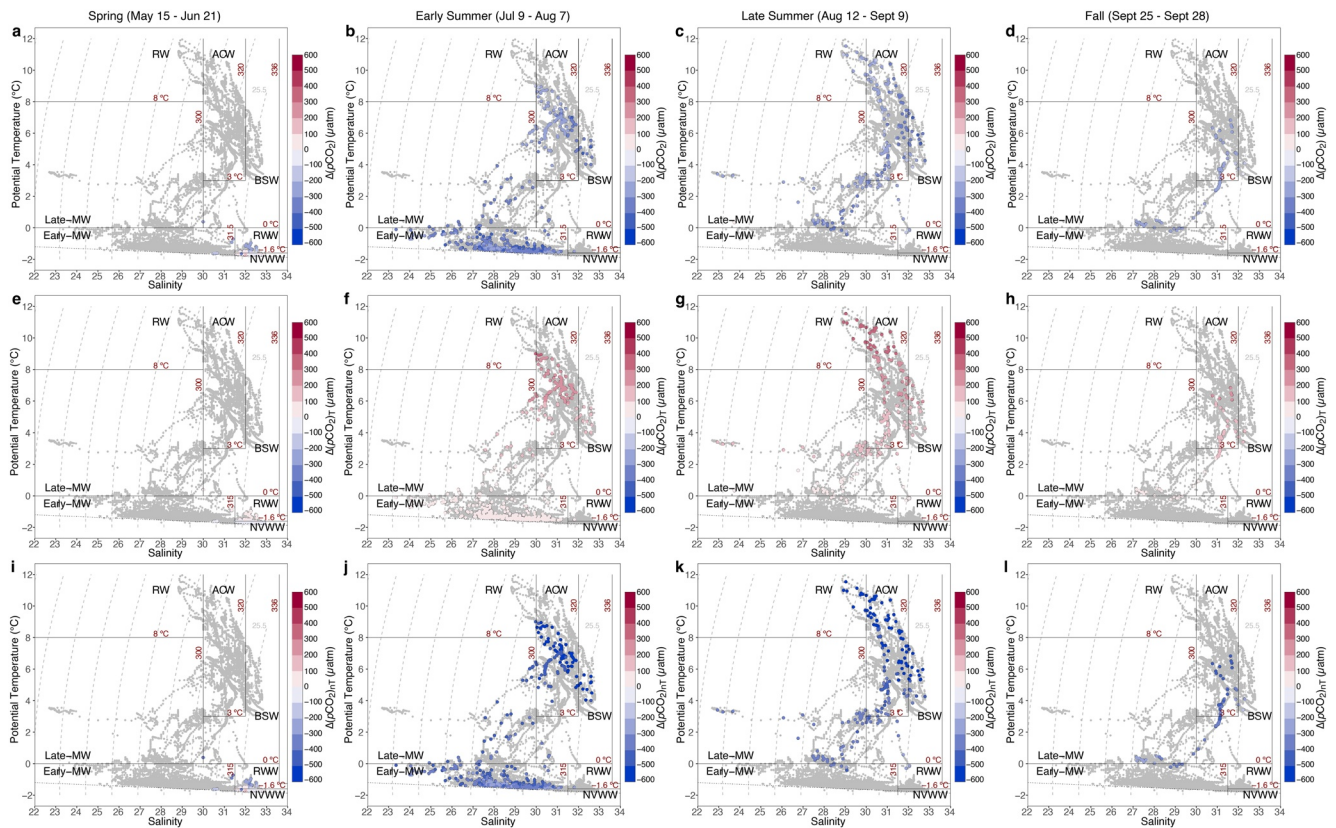


Figure 10. T/S diagram for sea surface $p\text{CO}_2$ in the Chukchi Sea in different seasons. The gray dots represent all underway measurements and colored dots denote the gridded $p\text{CO}_2$ (0.25° latitude \times 0.25° longitude) (a–d) $p\text{CO}_2$ difference between initial $p\text{CO}_2$ under the ice (i.e., $538 \mu\text{atm}$) and observed $p\text{CO}_2$ (e–g) potential $p\text{CO}_2$ changes induced by thermal effects, and (h–l) $p\text{CO}_2$ changes induced by non-thermal effects. The approximate water mass boundaries are denoted by solid lines. NVWW is newly-ventilated winter water; RW is remnant winter water; BSW is Bering summer water; ACW is Alaskan coastal water; MW is meltwater; RW is river water. The freezing line is indicated by the dashed line.

and $0.94 \pm 0.21 \mu\text{M}$ in the southern and northern Chukchi Sea, respectively (Table 5), nPO_4^{3-} -based NCP was estimated to be 0.41 ± 0.04 and $0.48 \pm 0.11 \text{ mmol P m}^{-2} \text{ d}^{-1}$ in the southern and northern Chukchi Sea, respectively (Table 5). Given a M C:N:P uptake ratio of 106:16:1 (Redfield, 1958), nNO_3^- -based NCP was estimated to be 23.2 ± 0.5 and $33.4 \pm 5.3 \text{ mmol C m}^{-2} \text{ d}^{-1}$ in the southern and northern Chukchi Sea. The analogous rates for nPO_4^{3-} -based NCP were 43.3 ± 4.0 and $50.9 \pm 11.3 \text{ mmol C m}^{-2} \text{ d}^{-1}$, respectively. Thus, the nDIC -based NCP was significantly higher than the NCP derived from nNO_3^- consumption by 66%–84% and was close to or slightly higher than nPO_4^{3-} -based NCP (Table 5). Although river runoff or precipitation may dominate endmembers in some locations and give different NCP estimates, it still cannot reconcile discrepancy in NCPs (Text S2 and Table S2 in Supporting Information S1). Therefore, other processes must add nutrients or remove DIC, or a novel, unaccounted for mechanism is required to explain this disparity.

N_2 fixation could be one possible process providing new nitrogen to the system and would reconcile the inconsistency between the NCP estimates (Park et al., 2008). Recent studies have shown that N_2 fixation can occur at low temperatures and high latitudes (Harding et al., 2018; Mills et al., 2018; Shiozaki et al., 2018; Sipler et al., 2017), which challenges the historical views that N_2 fixation is a warm-water process constrained to subtropical and tropical oligotrophic areas (von Friesen and Riemann, 2020; Zehr & Capone, 2020). Shiozaki et al. (2018) reported the N_2 fixation rates of 0.08 – $3.60 \text{ nmol N L}^{-1} \text{ d}^{-1}$ during late summer in 2015 in the Chukchi Sea, which is equivalent to 0.002 – $0.09 \text{ mmol N m}^{-2} \text{ d}^{-1}$ integrated over the top 25 m. Accounting for such a new source of nitrogen (using the upper limit), nNO_3^- -based NCP would slightly increase by only $\sim 2\%$, to 3.60 ± 0.07 and $5.15 \pm 0.80 \text{ mmol N m}^{-2} \text{ d}^{-1}$ in the southern and northern Chukchi Sea, respectively (Table 5). Thus, N_2 fixation cannot explain the inconsistencies in NCP estimates based on the deficits of nDIC and nNO_3^- .

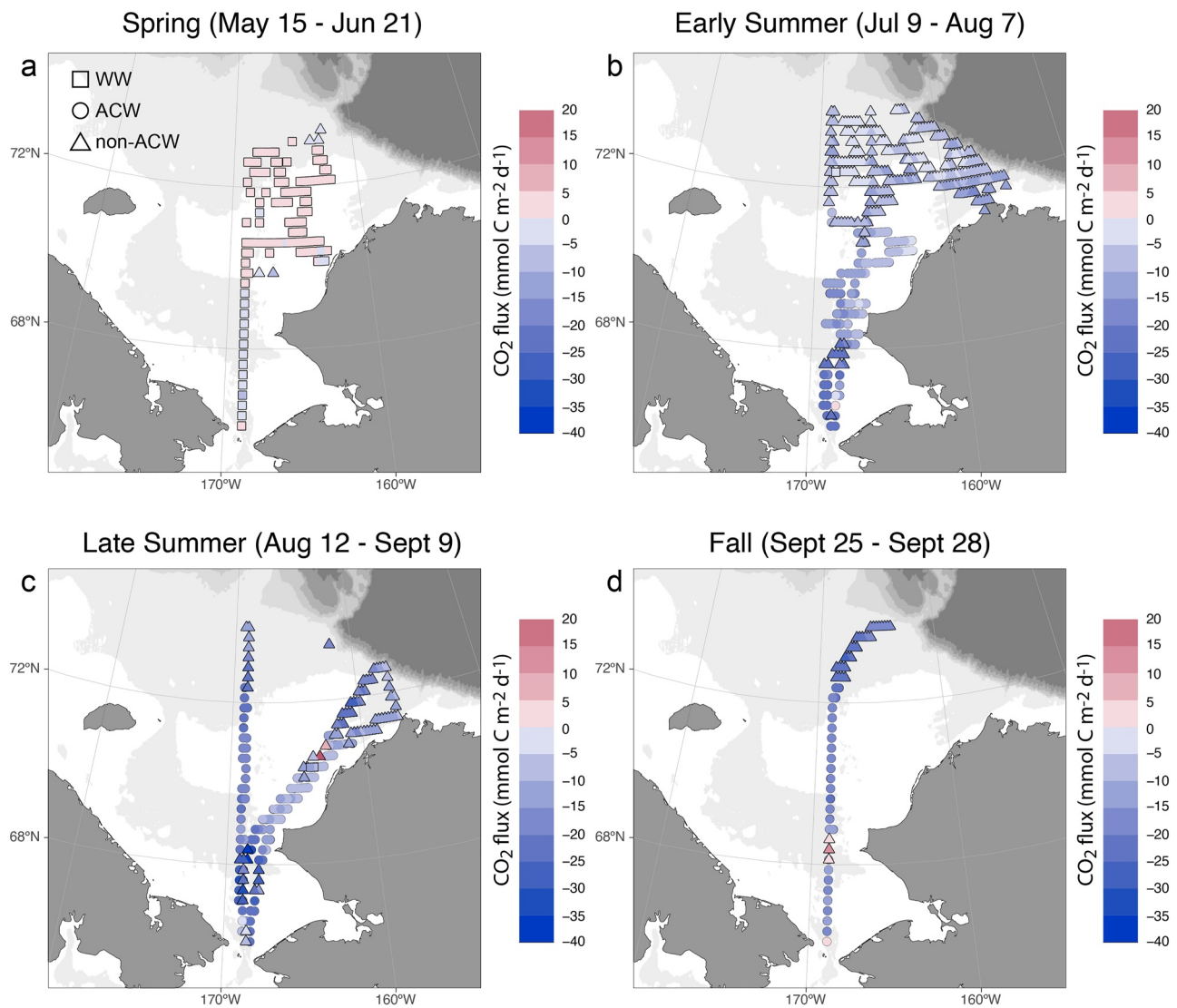


Figure 11. Seasonal variation in air-sea CO₂ flux in the Chukchi Sea in 2014. CO₂ flux were derived from gridded pCO₂ data (0.25° × 0.25°). Negative values of CO₂ flux values indicate that CO₂ uptake from the atmosphere. Square, circle and triangle represent winter water (Newly-Ventilated Winter Water and remnant winter water), Alaska coastal water (ACW and river water), and non-Alaska coastal water (Bering summer water and meltwater), respectively.

Table 4
Seasonal Variations in CO₂ Flux (mmol m⁻² d⁻¹) in the Chukchi Sea

Periods	Southern Chukchi sea (<69.5°N)			Northern Chukchi sea (>69.5°N)		
	Regional mean	ACW	Non-ACW	Regional mean	ACW	Non-ACW
Spring	-2.5 ± 1.5 (n = 15)	NA	NA	1.1 ± 1.1 (n = 145)	NA	-2.2 ± 2.4 (n = 6)
Early Summer	-15.9 ± 6.0 (n = 73)	-14.8 ± 5.7 (n = 62)	-22.3 ± 1.9 (n = 11) ^c	-7.2 ± 3.4 (n = 377)	-8.8 ± 2.6 (n = 58)	-7.0 ± 3.4 (n = 319) ^c
Late Summer	-18.3 ± 8.9 (n = 75)	-16.7 ± 8.1 (n = 59)	-24.3 ± 9.6 (n = 16) ^b	-13.3 ± 6.6 (n = 117)	-12.5 ± 5.5 (n = 54)	-14.2 ± 7.4 (n = 63)
Fall	-10.5 ± 8.4 (n = 17)	-13.7 ± 4.4 (n = 14)	4.4 ± 6.1 (n = 3) ^a	-21.1 ± 2.9 (n = 47)	-19.8 ± 1.8 (n = 15)	-21.7 ± 3.2 (n = 32) ^a

Note. We estimated CO₂ fluxes separately in two types of water masses: the ACW (including RW) and non-ACW (including BSW and MW but excluding NVWW and RW) for each season. Footnotes indicates if the mean of CO₂ flux in the non-ACW is statistically different from that in the ACW (t-test).

^ap < 0.05. ^bp < 0.01. ^cp < 0.001.

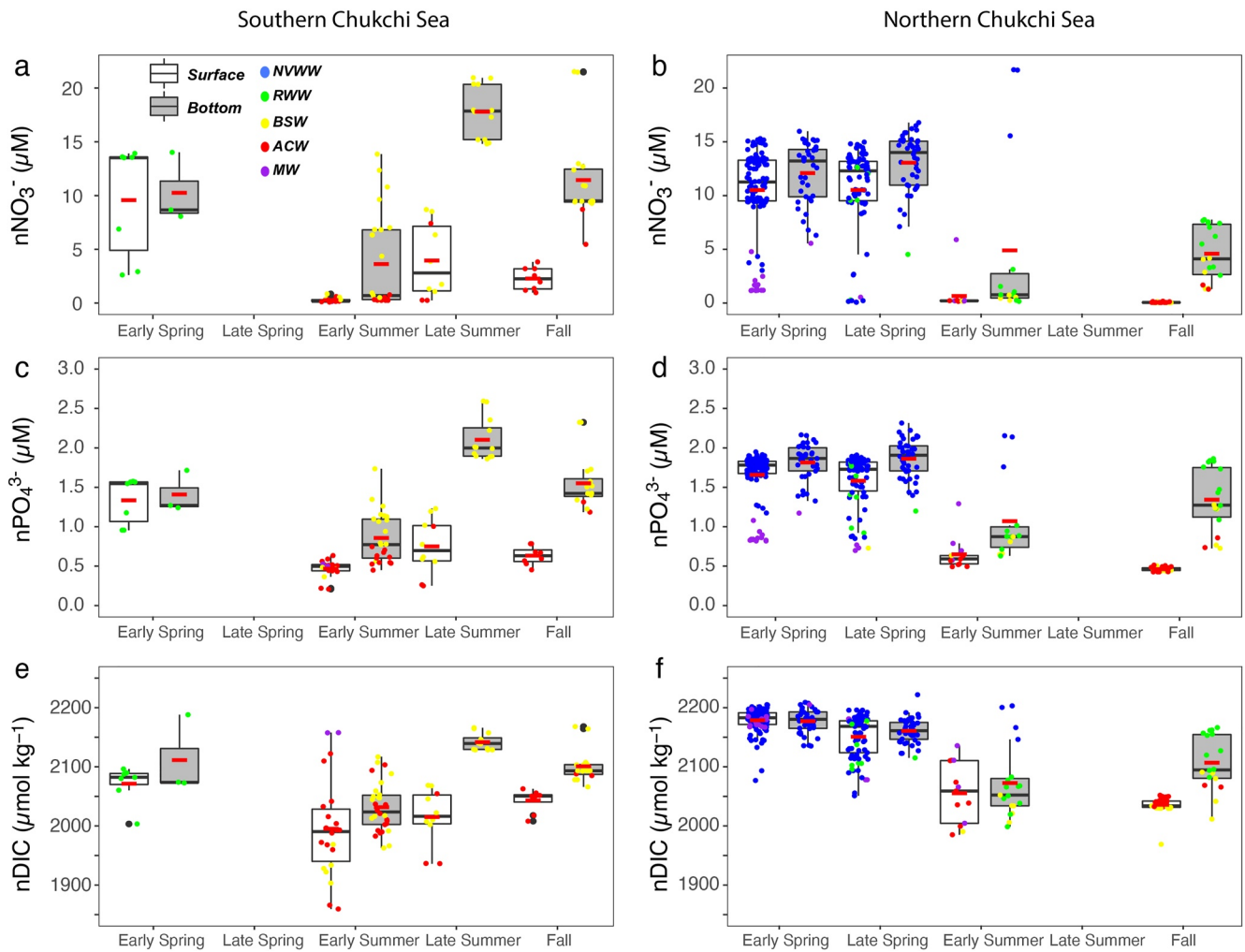


Figure 12. Seasonal variations of $n\text{NO}_3^-$, $n\text{PO}_4^{3-}$, and $n\text{DIC}$ and in the southern ($<69.5^\circ\text{N}$; a, c, and e) and northern Chukchi Sea ($>69.5^\circ\text{N}$; b, d and f). White and gray boxplots indicate data collected in the surface and bottom layers, respectively. Black and red bars within boxplots indicate medians and means, respectively. Individual measurements are also shown and color-coded by different water masses.

Table 5

Net Community Production Estimates in the Surface Mixed Layer Based on $n\text{DIC}$, $n\text{NO}_3^-$ and $n\text{PO}_4^{3-}$ Changes for the Period Between the Spring and the Early Summer of 2014 in the Chukchi Sea

Location	Δ (nTA)	Δ (nDIC)	Δ ($n\text{NO}_3^-$)	Δ ($n\text{PO}_4^{3-}$)	Growing season d	NCP-nDIC mmol C $\text{m}^{-2} \text{d}^{-1}$	NCP- $n\text{NO}_3^-$		NCP- $n\text{PO}_4^{3-}$		C:N uptake ratio	C:P uptake ratio	
	$\mu\text{mol kg}^{-1}$	$\mu\text{mol kg}^{-1}$	μM	μM			mmol N $\text{m}^{-2} \text{d}^{-1}$	mmol C $\text{m}^{-2} \text{d}^{-1}$	mmol P $\text{m}^{-2} \text{d}^{-1}$	mmol C $\text{m}^{-2} \text{d}^{-1}$			
Southern	-34 ± 37	79 ± 87	10.24 ± 0.20	1.19 ± 0.11	73	18	38.4 ± 26.2	3.51 ± 0.07	23.2 ± 0.5^a	0.41 ± 0.04	43.3 ± 4.0	10.9	94.0
Northern	-36 ± 34	95 ± 51	9.92 ± 1.57	0.94 ± 0.21	49	13	61.4 ± 20.0	5.06 ± 0.80	33.4 ± 5.3^b	0.48 ± 0.11	50.9 ± 11.3	12.1	128.0

Note. Differences in nTA, nDIC, $n\text{NO}_3^-$ and $n\text{PO}_4^{3-}$ were calculated as $\text{Variable}_{\text{spring}} - \text{Variable}_{\text{early summer}}$, thus negative values indicate an increase in variable in the later season. Nutrient-based NCP were converted to carbon (C) units assuming a Redfield M C:N:P uptake ratio of 106:16:1. C:N and C:P uptake ratios are defined as NCP_{nDIC} : NCP- $n\text{NO}_3^-$ and NCP_{nDIC} : NCP- $n\text{PO}_4^{3-}$. Footnotes indicates if the mean of NCP- $n\text{NO}_3^-$ and NCP- $n\text{PO}_4^{3-}$ in unit of $\text{mmol C m}^{-2} \text{d}^{-1}$ are statistically different than that in NCP nDIC (t-test).

^a $p < 0.05$. ^b $p < 0.01$.

CaCO₃ formation or bio-calcification would also contribute to DIC removal in the water column. However, a net increase in nTA in both southern and northern Chukchi Sea (Table 5) suggests that CaCO₃ dissolution (e.g., mineral ikaite in ice) may dominate TA dynamics, which actually adds more DIC in the water column. By comparing the NCP results of with or without CaCO₃ dissolution correction, we further estimated that CaCO₃ dissolution accounted for ~2.6% and 11.0% NCP_{-nDIC based} in the southern and northern Chukchi Seas, respectively, during the period between spring and early summer. Thus, CaCO₃ dissolution cannot explain the inconsistencies in NCP estimates either.

An alternative explanation is that, during intensive primary production, phytoplankton carbon and nutrient uptake in the Chukchi Sea are non-Redfieldian; DIC uptake exceeds that expected for the observed N and P uptake. Based on deficits of nDIC and n PO₄³⁻, we found that C:P uptake ratio only slightly deviated from the Redfield ratio around 94.0–128.0 (Table 5). Since the remaining PO₄³⁻ (~0.5 μM) would not limit phytoplankton growth, the inconsistency in NCP must be attributable to a non-Redfield C:N uptake behavior. We found that phytoplankton growth in a N-limited surface water led to a C:N uptake ratio of about 10.9–12.1 (Table 5), which is close to the measurements of the particulate organic C:N ratio in the Chukchi Sea in the summer of 2002 (C:N ratio >9; Bates et al., 2005), but much higher than the Redfield ratio and the observed annual mean of particulate organic C:N ratio (~6.4; Frigstad et al., 2014). We attribute this disagreement to a rapid seasonal change in the phytoplankton C:N uptake ratio or an ecological response. The high NCP during late spring throughout early summer makes the Chukchi Sea an extremely NO₃⁻-limited ecosystem (Brown et al., 2015; Codispoti et al., 2013; Mills et al., 2015; Zheng et al., 2021), resulting in a higher C:N uptake ratio and hence a higher particulate organic C:N ratio (Bates et al., 2005). In contrast, the C:N uptake ratio is relatively low (close to the Redfield ratio) in early spring (Bates et al., 2005) and fall (Frigstad et al., 2014) when NO₃⁻ is replenished.

Additional evidence for C:N variability comes from water column-integrated NCP estimates. As phytoplankton growth and nutrient consumption may erode the nitricline, NCP calculated from surface water depletion of NO₃⁻ and DIC probably underestimates the true NCP or overestimates the C:N uptake ratio, we computed depth-integrated NCP for the entire water column. Previously, phytoplankton growth was observed in bottom waters in the southern Chukchi Sea in summers of 2010 and 2011 (Brown et al., 2015). In 2014, we observed excessive consumption of NO₃⁻ in bottom waters not only in the southern Chukchi Sea, but also in the northern part (Figures 7h and 12b). The mean depth-integrated NCP in the southern and northern Chukchi Sea derived from nDIC changes were 65.4 ± 46.7 and 98.7 ± 55.8 mmol C m⁻² d⁻¹, and NCP derived from n NO₃⁻ changes were 5.3 ± 1.5 and 8.4 ± 4.9 mmol N m⁻² d⁻¹, respectively. These proportional increases in NCP estimates yield a C:N of 11.8–12.2, similar to that from the mixed layer analysis (Table S1 in Supporting Information S1), which confirms that C:N uptake ratio in the period between late spring and early summer was much higher than the Redfield ratio (C:N ~ 6.6). Given that nNO₃⁻ was still depleted in late summer and fall in the northern Chukchi Sea (Figure 12b), we further suggest that the C:N uptake ratio would remain high in the northern Chukchi Sea, while the C:N uptake ratio may return to the canonical Redfield ratio in the southern Chukchi Sea in the later season due to NO₃⁻ replenishment exceeding consumption (Frigstad et al., 2014; Zheng et al., 2021).

4.3. Flexible Stoichiometric C:N Uptake Ratio Enhances Air-Sea CO₂ Uptake

The Chukchi Sea has been identified as a N-limited ecosystem during the growing season (Brown et al., 2015; Codispoti et al., 2013; Mills et al., 2015; Zheng et al., 2021; Zhuang et al., 2020). Thus, DIC assimilation and associated NCP calculation is directly linked to the uptake of the most limited nutrient (NO₃⁻) and an assumption of a fixed C:N uptake ratio (Arrigo et al., 2017; Hansell et al., 1993). However, these assumptions are not always valid, especially when phytoplankton are experiencing N-limitation, because the internal C:N ratio of phytoplankton can deviate from the Redfield ratio (Finkel et al., 2010; Spilling et al., 2015) and the produced carbon-rich DOM can contribute a significant fraction of NCP (Baetge et al., 2020; Bif & Hansell, 2019). For example, when nutrients are sufficient, phytoplankton can assimilate and store extra nutrients for future use (i.e., luxury consumption; Elrifi & Turpin, 1985; Sommer, 1991). When nutrients in the internal pool or ambient water are not adequate, phytoplankton may release the fixed carbon as extracellular dissolved organic carbon (DOC) (Myklestad, 1995) or produce transparent exopolymeric particles (Mari et al., 2001; Vernet et al., 1998) and carbon-rich organic matter (Humphreys et al., 2019). From a biogeochemical perspective, this non-Redfield C:N uptake by phytoplankton may greatly impact seasonal variation in sea surface pCO₂ and air-sea CO₂ flux. For example, Fransner et al. (2018) found that CO₂ uptake from the atmosphere can be underestimated by 50% in

the northern Baltic Sea if a fixed Redfield ratio is used to determine carbon assimilation. However, there is little evidence for such a mechanism operating in the polar regions.

To demonstrate how a flexible C:N uptake stoichiometry by phytoplankton and possible CaCO_3 dissolution during active ice melting affect the air-sea CO_2 flux, we used a box model to reproduce sea surface $p\text{CO}_2$ in the Chukchi Sea from spring to early summer in 2014. Three simulations were performed; scenario 1 with a non-Redfield C:N uptake ratio corrected for CaCO_3 dissolution, scenario 2 with a non-Redfield C:N uptake ratio without correcting for CaCO_3 dissolution and scenario 3 with a fixed Redfield C:N ratio (Figure 13). In the simulation with a non-Redfield C:N uptake stoichiometry (scenario 1 & 2), more efficient DIC drawdown led to a lower DIC concentration during early summer when compared to the Redfield ratio scenario, which results in better agreement with observations in both the southern and northern Chukchi Sea (Figures 13c and 13d). Furthermore, the non-Redfield stoichiometry approach better reproduces observations of $p\text{CO}_2$ during this intensive growing season (Figures 13e and 13f), whereas carbon fixation in the fixed-stoichiometry (Redfield ratio) simulation is not efficient enough to counteract the effects of warming and air-sea CO_2 exchange on sea surface $p\text{CO}_2$. More importantly, the higher carbon fixation with a non-Redfield C:N uptake ratio, compared to the fixed Redfield uptake ratio, enhances air-sea CO_2 uptake in the Chukchi Sea. The net CO_2 uptake from the atmosphere in the non-Redfield stoichiometry scenario over the simulation period (day 136 to day 219 for the southern Chukchi Sea and day 167 to day 219 for the northern Chukchi Sea) is estimated to be $751 \text{ mmol C m}^{-2}$ and $343 \text{ mmol C m}^{-2}$, respectively, in the southern and northern Chukchi Sea, which are 42% and 85% higher than CO_2 uptake in the fixed-stoichiometry scenario ($528 \text{ mmol C m}^{-2}$ and $185 \text{ mmol C m}^{-2}$). Thus, we conclude that about 30%–46% of CO_2 uptake during this intensive growing season is supported by phytoplankton stoichiometric flexibility. By

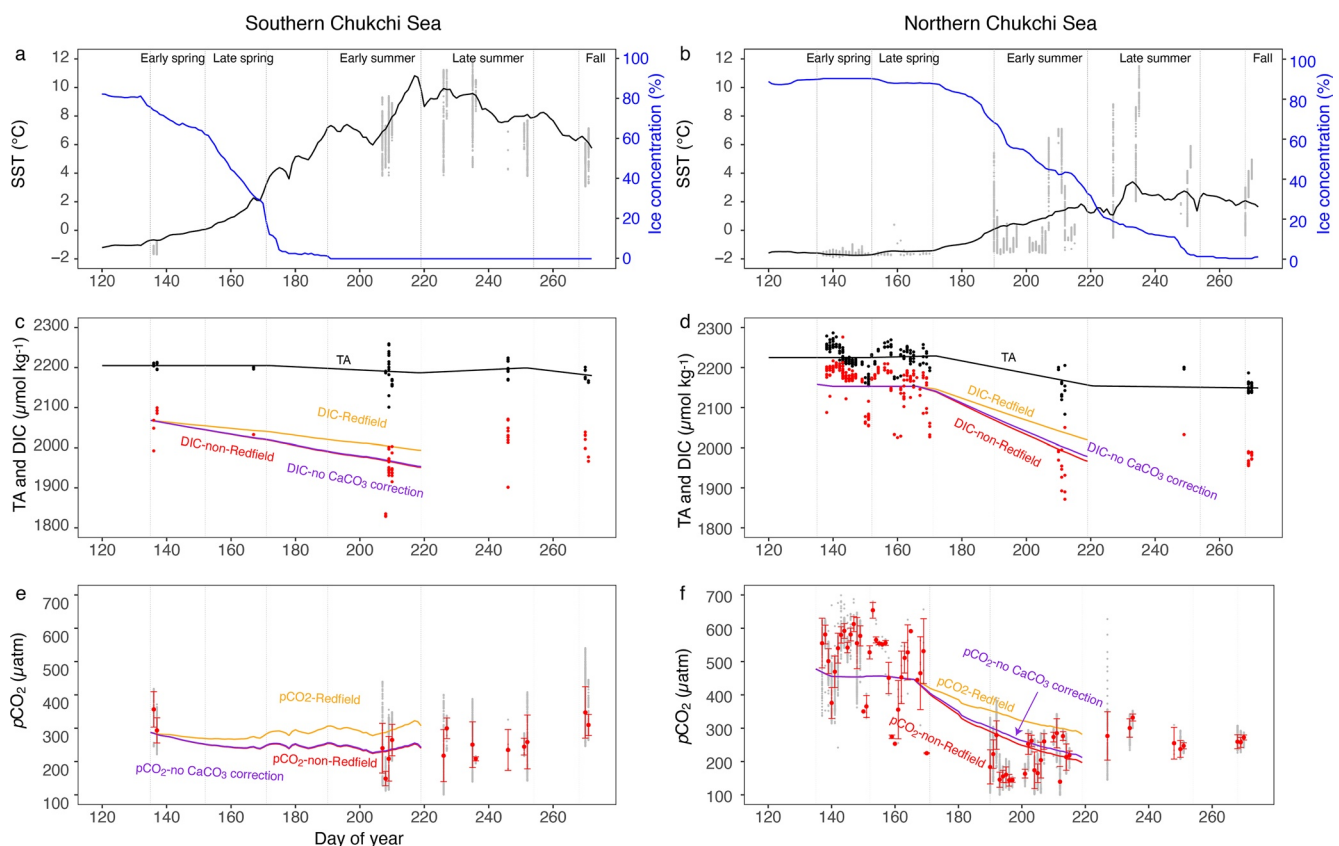


Figure 13. Observed and modeled seasonal variations in (a, b) Sea surface temperature (SST) and ice concentration (c, d) TA and dissolved inorganic carbon (DIC), and (e, f) $p\text{CO}_2$ in the southern Chukchi Sea (left column) and the northern Chukchi Sea (right column). The yellow lines are model results with fixed C:N uptake ratio (Redfield ratio). The red and purple lines indicate the model results with non-Redfield C:N uptake ratio with and without CaCO_3 dissolution correction, respectively. Black and red dots in c and d are discrete samples of TA and DIC, respectively. Gray dots are underway measurements of SST (a, b) and $p\text{CO}_2$ (e, f). Daily means with error bar (\pm standard deviation) of underway $p\text{CO}_2$ are presented in e and f. Five periods, including early and late spring, early and late summer, and fall are indicated by vertical dashed lines.

comparing the results of scenarios 1 and 2, we further quantified that the correction of CaCO₃ dissolution during ice melting from spring to early summer accounted for ~1% and 9% CO₂ uptake in the southern and northern Chukchi Sea, respectively, which is a significant fraction of NCP estimate. The difference in the net uptake of atmospheric CO₂ between these simulations could increase as nutrient-limited conditions and high C:N uptake mechanisms extend to a longer growing season (e.g., late summer and fall).

5. Summary

Seasonality of biogeochemical properties determines how an ocean ecosystem responds to external and internal forcings. By synthesizing a rare data set of underway measurements and discrete samples collected in five consecutive cruises in 2014, we presented a complete seasonal cycle (covering spring through fall) of sea surface pCO₂ and biogeochemical properties in the Chukchi Sea.

We first explored the dominant drivers of seasonal pCO₂ change as water masses evolve, revealing that thermal and non-thermal effects have different impacts on sea surface pCO₂ and air-sea CO₂ fluxes in different water masses. The non-ACW with stronger biological CO₂ removal and a weaker warming effect has a stronger atmospheric CO₂ uptake potential in summer months than ACW does. We suggest that the Chukchi Sea will become a greater CO₂ sink in the future as the proportion of nutrient-rich non-ACW increases.

We then estimated NCP for the most intensive growing period (spring to early summer) using observed DIC and nutrient data, and found that carbon-based NCP was consistently higher than NO₃⁻-based NCP by 66%–84%. We attributed this inconsistency in NCP estimates to a non-Redfield uptake of carbon and nutrients.

To investigate this hypothesis, we performed two model simulations to test how a flexible stoichiometry of C:N uptake ratio can affect seasonal biogeochemical dynamics and air-sea CO₂ exchange. Comparing modeled results and observations, we show that a variable phytoplankton C:N stoichiometry is needed in order to better simulate and understand the seasonal biogeochemical dynamics and air-sea CO₂ exchange. In particular, this stoichiometric flexibility in phytoplankton enables more efficient DIC-fixation, which contributes about 30%–46% of CO₂ uptake from atmosphere in the Chukchi Sea. These model results also have important implications for biological pump estimates in the Chukchi ecosystem and parametrizing C and N cycles in regional biogeochemical models.

Conflict of Interest

The authors declare no conflicts of interest relevant to this study.

Data Availability Statement

All the data are archived in publicly accessible databases. The SOCAT data can be downloaded from <https://www.socat.info/index.php/data-access/>. The data of discrete sample of carbonate chemistry, nutrients, dissolved oxygen and Chl *a* are also archived in publicly accessible databases (<https://arcticdata.io/catalog/view/doi%3A10.18739%2FA21C1TG6R>; <https://data.mendeley.com/datasets/dfpxxwm24c/2>; and <http://www.godac.jamstec.go.jp/darwin/cruise/mirai/mr14-05/e>). The model simulation data is also accessible via <https://data.mendeley.com/datasets/xhj79xjhp/1>.

References

- Ardyna, M., & Arrigo, K. R. (2020). Phytoplankton dynamics in a changing Arctic Ocean. *Nature Climate Change*, *10*(10), 892–903. <https://doi.org/10.1038/s41558-020-0905-y>
- Armstrong, F., Stearns, C. R., & Strickland, J. (1967). The measurement of upwelling and subsequent biological process by means of the Technicon Autoanalyzer® and associated equipment. *Deep-Sea Research*, *14*(3), 381–389. [https://doi.org/10.1016/0011-7471\(67\)90082-4](https://doi.org/10.1016/0011-7471(67)90082-4)
- Arrigo, K. R., Mills, M. M., van Dijken, G. L., Lowry, K. E., Pickart, R. S., & Schlitzer, R. (2017). Late spring nitrate distributions beneath the ice-covered northeastern Chukchi Shelf. *Journal of Geophysical Research: Biogeosciences*, *122*(9), 2409–2417. <https://doi.org/10.1002/2017jg003881>
- Arrigo, K. R., & van Dijken, G. L. (2015). Continued increases in Arctic Ocean primary production. *Progress in Oceanography*, *136*, 60–70. <https://doi.org/10.1016/j.pocan.2015.05.002>
- Baetge, N., Graff, J. R., Behrenfeld, M. J., & Carlson, C. A. (2020). Net community production, dissolved organic carbon accumulation, and vertical export in the Western North Atlantic. *Frontiers in Marine Science*, *7*, 227. <https://doi.org/10.3389/fmars.2020.00227>
- Bakker, D. C., Pfeil, B., Landa, C. S., Metzl, N., O'Brien, K. M., Olsen, A., et al. (2016). A multi-decade record of high-quality fCO₂ data in version 3 of the Surface Ocean CO₂ Atlas (SOCAT). *Earth System Science Data*, *8*(2), 383–413. <https://doi.org/10.5194/essd-8-383-2016>

Acknowledgments

This work was supported by the United States National Science Foundation (PLR-1304337 and OPP-1926158), the US National Aeronautics and Space Administration (80NSSC22K0151), the National Key Research and Development Program of China (2019YFE0114800), the National Science Foundation of China (42176230, 41941013), the Green Network of Excellence (GRENE) Program/Arctic Climate Change Research Project, Arctic Challenge for Sustainability (ArCS; JPMXD1300000000) and Arctic Challenge for Sustainability II (ArCS II; JPMXD1420318865) Projects, which were funded by the Ministry of Education, Culture, Sports, Science and Technology of Japan (MEXT).

- Bates, N. R., Cai, W. J., & Mathis, J. T. (2011). The ocean carbon cycle in the western Arctic Ocean: Distributions and air-sea fluxes of carbon dioxide. *Oceanography*, 24(3), 186–201. <https://doi.org/10.5670/oceanog.2011.71>
- Bates, N. R., Hansell, D. A., Moran, S. B., & Codispoti, L. A. (2005). Seasonal and spatial distribution of particulate organic matter (POM) in the Chukchi and Beaufort Seas. *Deep Sea Research Part II: Topical Studies in Oceanography*, 52(24–26), 3324–3343. <https://doi.org/10.1016/j.dsr2.2005.10.003>
- Bif, M. B., & Hansell, D. A. (2019). Seasonality of dissolved organic carbon in the upper Northeast Pacific Ocean. *Global Biogeochemical Cycles*, 33(5), 526–539. <https://doi.org/10.1029/2018gb006152>
- Brewer, P. G., & Goldman, J. C. (1976). Alkalinity changes generated by phytoplankton growth. *Limnology & Oceanography*, 21(1), 108–117. <https://doi.org/10.4319/lo.1976.21.1.0108>
- Brown, Z. W., Casciotti, K. L., Pickart, R. S., Swift, J. H., & Arrigo, K. R. (2015). Aspects of the marine nitrogen cycle of the Chukchi Sea shelf and Canada Basin. *Deep Sea Research Part II: Topical Studies in Oceanography*, 118, 73–87. <https://doi.org/10.1016/j.dsr2.2015.02.009>
- Buchanan, P. J., Matear, R. J., Chase, Z., Phipps, S. J., & Bindoff, N. L. (2018). Dynamic biological functioning important for simulating and stabilizing ocean biogeochemistry. *Global Biogeochemical Cycles*, 32(4), 565–593. <https://doi.org/10.1002/2017gb005753>
- Buck, A. L. (1981). New equations for computing vapor pressure and enhancement factor. *Journal of Applied Meteorology and Climatology*, 20(12), 1527–1532. [https://doi.org/10.1175/1520-0450\(1981\)020<1527:necvcp>2.0.co;2](https://doi.org/10.1175/1520-0450(1981)020<1527:necvcp>2.0.co;2)
- Cai, W. J., Chen, L., Chen, B., Gao, Z., Lee, S. H., Chen, J., et al. (2010). Decrease in the CO₂ uptake capacity in an ice-free Arctic Ocean basin. *Science*, 329(5991), 556–559. <https://doi.org/10.1126/science.1189338>
- Chen, B., Cai, W. J., & Chen, L. (2015). The marine carbonate system of the Arctic Ocean: Assessment of internal consistency and sampling considerations, summer 2010. *Marine Chemistry*, 176, 174–188. <https://doi.org/10.1016/j.marchem.2015.09.007>
- Clark, S. C., Granger, J., Mastorakis, A., Aguilar-Islas, A., & Hastings, M. G. (2020). An investigation into the origin of nitrate in Arctic sea ice. *Global Biogeochemical Cycles*, 34(2), e2019GB006279. <https://doi.org/10.1029/2019gb006279>
- Codispoti, L. A., Kelly, V., Thessen, A., Matrai, P., Suttles, S., Hill, V., et al. (2013). Synthesis of primary production in the Arctic Ocean: III. Nitrate and phosphate based estimates of net community production. *Progress in Oceanography*, 110, 126–150. <https://doi.org/10.1016/j.pocean.2012.11.006>
- Comiso, J. C. (2017). *Bootstrap sea ice concentrations from Nimbus-7 SMMR and DMSP SSM/I-SSMIS, version 3*. NASA National Snow and Ice Data Center Distributed Active Archive Center. <https://doi.org/10.5067/7Q8HCCWS4I0R>
- Corlett, W. B., & Pickart, R. S. (2017). The Chukchi slope current. *Progress in Oceanography*, 153, 50–65. <https://doi.org/10.1016/j.pocean.2017.04.005>
- Dickson, A. G. (1996). Determination of dissolved oxygen in sea water by Winkler titration. *WOCE Operations Manual*, Section 3.1, Part 3.1.3 WHP Operations and Methods, WHP Office Report WHPO 91-1, WOCE Report No. 68/91, November 1994, Revision 1, 3, 1–13. Retrieved from https://www.nodc.noaa.gov/woce/woce_v3/wocedata_1/whp/manuals/pdf/91_1/dick-%20son2.pdf
- Dickson, A. G., Sabine, C. L., & Christian, J. R. (2007). *Guide to best practices for ocean CO₂ measurements*. North Pacific Marine Science Organization.
- Elrifi, I. R., & Turpin, D. H. (1985). Steady-state luxury consumption and the concept of optimum nutrient ratios: A study with phosphate and nitrate limited *Selenastrum minutum* (chlorophyta) 1. *Journal of Phycology*, 21(4), 592–602. <https://doi.org/10.1111/j.0022-3646.1985.00592.x>
- Evans, W., Mathis, J., Cross, J., Bates, N., Frey, K., Else, B., et al. (2015). Sea-air CO₂ exchange in the western Arctic coastal ocean. *Global Biogeochemical Cycles*, 29(8), 1190–1209. <https://doi.org/10.1002/2015gb005153>
- Fetterer, F., Knowles, K., Meier, W. N., Savoie, M., & Windnagel, A. K. (2017). Updated daily. *Sea ice index*, Version 3. NSIDC: National Snow and Ice Data Center. <https://doi.org/10.7265/NSK072F8>
- Finkel, Z. V., Beardall, J., Flynn, K. J., Quigg, A., Rees, T. A. V., & Raven, J. A. (2010). Phytoplankton in a changing world: Cell size and elemental stoichiometry. *Journal of Plankton Research*, 32(1), 119–137. <https://doi.org/10.1093/plankt/fbp098>
- Fransser, F., Gustafsson, E., Tedesco, L., Vichii, M., Hordoir, R., Roquet, F., et al. (2018). Non-redfieldian dynamics explain seasonal pCO₂ drawdown in the Gulf of Bothnia. *Journal of Geophysical Research: Oceans*, 123(1), 166–188. <https://doi.org/10.1002/2017jc013019>
- Frigstad, H., Andersen, T., Bellerby, R. G., Silyakova, A., & Hessen, D. O. (2014). Variation in the seston C:N ratio of the Arctic Ocean and pan-Arctic shelves. *Journal of Marine Systems*, 129, 214–223. <https://doi.org/10.1016/j.jmarsys.2013.06.004>
- Friis, K., Körtzinger, A., & Wallace, D. W. (2003). The salinity normalization of marine inorganic carbon chemistry data. *Geophysical Research Letters*, 30(2). <https://doi.org/10.1029/2002gl015898>
- Gattuso, J.-P., Epitalon, J.-M., Lavigne, H., & Orr, J. (2018). Seacarb: Seawater carbonate chemistry. R package version 3.2.10. Retrieved from <http://CRAN.R-project.org/package=seacarb>
- Gong, D., & Pickart, R. S. (2015). Summertime circulation in the eastern Chukchi Sea. *Deep Sea Research Part II: Topical Studies in Oceanography*, 118, 18–31. <https://doi.org/10.1016/j.dsr2.2015.02.006>
- Grebmeier, J. M., Bluhm, B. A., Cooper, L. W., Danielson, S. L., Arrigo, K. R., Blanchard, A. L., et al. (2015). Ecosystem characteristics and processes facilitating persistent macrobenthic biomass hotspots and associated benthivory in the Pacific Arctic. *Progress in Oceanography*, 136, 92–114. <https://doi.org/10.1016/j.pocean.2015.05.006>
- Hansell, D. A., Whittledge, T. E., & Goering, J. J. (1993). Patterns of nitrate utilization and new production over the Bering-Chukchi shelf. *Continental Shelf Research*, 13(5–6), 601–627. [https://doi.org/10.1016/0278-4343\(93\)90096-g](https://doi.org/10.1016/0278-4343(93)90096-g)
- Harding, K., Turk-Kubo, K. A., Sipler, R. E., Mills, M. M., Bronk, D. A., & Zehr, J. P. (2018). Symbiotic unicellular cyanobacteria fix nitrogen in the Arctic Ocean. *Proceedings of the National Academy of Sciences*, 115(52), 13371–13375. <https://doi.org/10.1073/pnas.1813658115>
- Holm-Hansen, O., Lorenzen, C. J., Holmes, R. W., & Strickland, J. D. H. (1965). Fluorometric determination of chlorophyll. *ICES. Journal of Marine Science*, 30(1), 3–15. <https://doi.org/10.1093/icesjms/30.1.3>
- Humphreys, M. P., Achterberg, E. P., Hopkins, J. E., Chowdhury, M. Z., Griffiths, A. M., Hartman, S. E., et al. (2019). Mechanisms for a nutrient-conserving carbon pump in a seasonally stratified, temperate continental shelf sea. *Progress in Oceanography*, 177, 101961. <https://doi.org/10.1016/j.pocean.2018.05.001>
- Hydes, D. J., Aoyama, M., Aminot, A., Bakker, K., Becker, S., Coverly, S., et al. (2010). Determination of dissolved nutrients (N, P, Si) in seawater with high precision and inter-comparability using gas-segmented continuous flow analysers. In E. M. Hood, C. L. Sabine, & B. M. Sloyan (Eds.), *The GO-SHIP Repeat Hydrography manual: A collection of Expert reports and guidelines (IOCCP report number 14, ICPO publication series Number 134, pp. 1–87)*. UNESCO-IOC. Retrieved from <http://www.go-ship.org/HydroMan.html>
- Jiang, L.-Q., Cai, W.-J., & Wang, Y. (2008). A comparative study of carbon dioxide in river- and marine-dominated estuaries. *Limnology & Oceanography*, 53(6), 2603–2615. <https://doi.org/10.4319/lo.2008.53.6.2603>
- Kawaguchi, Y., Nishino, S., & Inoue, J. (2015). Fixed-point observation of mixed layer evolution in the seasonally ice-free Chukchi Sea: Turbulent mixing due to gale winds and internal gravity waves. *Journal of Physical Oceanography*, 45(3), 836–853. <https://doi.org/10.1175/jpo-d-14-0149.1>

- Koeve, W. (2006). C:N stoichiometry of the biological pump in the north Atlantic: Constraints from climatological data. *Global Biogeochemical Cycles*, 20(3). <https://doi.org/10.1029/2004gb002407>
- Kwiatkowski, L., Aumont, O., Bopp, L., & Ciais, P. (2018). The impact of variable phytoplankton stoichiometry on projections of primary production, food quality, and carbon uptake in the global ocean. *Global Biogeochemical Cycles*, 32(4), 516–528. <https://doi.org/10.1002/2017gb005799>
- Lee, K. (2001). Global net community production estimated from the annual cycle of surface water total dissolved inorganic carbon. *Limnology & Oceanography*, 46(6), 1287–1297. <https://doi.org/10.4319/lo.2001.46.6.1287>
- Lewis, K. M., van Dijken, G. L., & Arrigo, K. R. (2020). Changes in phytoplankton concentration now drive increased Arctic Ocean primary production. *Science*, 369(6500), 198–202. <https://doi.org/10.1126/science.aay8380>
- Li, M., Pickart, R. S., Spall, M. A., Weingartner, T. J., Lin, P., Moore, G. W. K., & Qi, Y. (2019). Circulation of the Chukchi Sea shelfbreak and slope from moored timeseries. *Progress in Oceanography*, 172, 14–33. <https://doi.org/10.1016/j.pocean.2019.01.002>
- Lin, P., Pickart, R. S., McRaven, L. T., Arrigo, K. R., Bahr, F., Lowry, K. E., et al. (2019). Water mass evolution and circulation of the northeastern Chukchi Sea in summer: Implications for nutrient distributions. *Journal of Geophysical Research: Oceans*, 124(7), 4416–4432. <https://doi.org/10.1029/2019JC015185>
- Lowry, K. E., Pickart, R. S., Mills, M. M., Brown, Z. W., van Dijken, G. L., Bates, N. R., & Arrigo, K. R. (2015). The influence of winter water on phytoplankton blooms in the Chukchi Sea. *Deep-Sea Research Part II Topical Studies in Oceanography*, 118, 53–72. <https://doi.org/10.1016/j.dsr2.2015.06.006>
- Mari, X., Beauvais, S., Lemée, R., & Pedrotti, M. L. (2001). Non-redfield C:N ratio of transparent exopolymeric particles in the northwestern Mediterranean Sea. *Limnology & Oceanography*, 46(7), 1831–1836. <https://doi.org/10.4319/lo.2001.46.7.1831>
- Martiny, A. C., Vrugt, J. A., Primeau, F. W., & Lomas, M. W. (2013). Regional variation in the particulate organic carbon to nitrogen ratio in the surface ocean. *Global Biogeochemical Cycles*, 27(3), 723–731. <https://doi.org/10.1002/gbc.20061>
- Mathis, J. T., Bates, N. R., Hansell, D. A., & Babila, T. (2009). Net community production in the northeastern Chukchi Sea. *Deep Sea Research Part II: Topical Studies in Oceanography*, 56(17), 1213–1222. <https://doi.org/10.1016/j.dsr2.2008.10.017>
- Meredith, M., & Sommerkorn, M. (2019). *IPCC special report on the ocean and cryosphere in a changing climate (SROCC)*, Chapter 3 IPCC.
- Millero, F. J., Graham, T. B., Huang, F., Bustos-Serrano, H., & Pierrot, D. (2006). Dissociation constants of carbonic acid in seawater as a function of salinity and temperature. *Marine Chemistry*, 100(1–2), 80–94. <https://doi.org/10.1016/j.marchem.2005.12.001>
- Mills, M. M., Brown, Z. W., Laney, S. R., Ortega-Retuerta, E., Lowry, K. E., Van Dijken, G. L., & Arrigo, K. R. (2018). Nitrogen limitation of the summer phytoplankton and heterotrophic prokaryote communities in the Chukchi Sea. *Frontiers in Marine Science*, 5, 362. <https://doi.org/10.3389/fmars.2018.00362>
- Mills, M. M., Brown, Z. W., Lowry, K. E., van Dijken, G. L., Becker, S., Pal, S., et al. (2015). Impacts of low phytoplankton NO₃⁻: PO₄₃⁻ utilization ratios over the Chukchi Shelf, Arctic Ocean. *Deep Sea Research Part II: Topical Studies in Oceanography*, 118, 105–121. <https://doi.org/10.1016/j.dsr2.2015.02.007>
- Myklestad, S. M. (1995). Release of extracellular products by phytoplankton with special emphasis on polysaccharides. *Science of the Total Environment*, 165(1–3), 155–164. [https://doi.org/10.1016/0048-9697\(95\)04549-g](https://doi.org/10.1016/0048-9697(95)04549-g)
- Nishino, S., Kawaguchi, Y., Inoue, J., Hirawake, T., Fujiwara, A., Futsuki, R., et al. (2015). Nutrient supply and biological response to wind-induced mixing, inertial motion, internal waves, and currents in the northern Chukchi Sea. *Journal of Geophysical Research: Oceans*, 120(3), 1975–1992. <https://doi.org/10.1002/2014jc010407>
- Nishino, S., Kawaguchi, Y., Inoue, J., Yamamoto-Kawai, M., Aoyama, M., Harada, N., & Kikuchi, T. (2020). Do strong winds impact water mass, nutrient, and phytoplankton distributions in the ice-free Canada basin in the fall? *Journal of Geophysical Research: Oceans*, 125(1), e2019JC015428. <https://doi.org/10.1029/2019jc015428>
- Onarheim, I. H., Eldevik, T., Smedsrud, L. H., & Stroeve, J. C. (2018). Seasonal and regional manifestation of Arctic sea ice loss. *Journal of Climate*, 31(12), 4917–4932. <https://doi.org/10.1175/jcli-d-17-0427.1>
- Ouyang, Z., Qi, D., Chen, L., Takahashi, T., Zhong, W., DeGrandpre, M. D., et al. (2020). Sea-ice loss amplifies summertime decadal CO₂ increase in the western Arctic Ocean. *Nature Climate Change*, 10(7), 678–684. <https://doi.org/10.1038/s41558-020-0784-2>
- Ouyang, Z., Qi, D., Zhong, W., Chen, L., Gao, Z., Lin, H., et al. (2021). Summertime evolution of net community production and CO₂ flux in the western Arctic Ocean. *Global Biogeochemical Cycles*, 35(3), e2020GB006651. <https://doi.org/10.1029/2020gb006651>
- Pacini, A., Moore, G. W. K., Pickart, R. S., Nobre, C., Bahr, F., Våge, K., & Arrigo, K. R. (2019). Characteristics and transformation of Pacific winter water on the Chukchi Sea shelf in late spring. *Journal of Geophysical Research: Oceans*, 124(10), 7153–7177. <https://doi.org/10.1029/2019jc015261>
- Park, G. H., Lee, K., Wanninkhof, R., Zhang, J. Z., Hansell, D. A., & Feely, R. A. (2008). Large, non-Redfieldian drawdown of nutrients and carbon in the extratropical North Atlantic Ocean (46°N): Evidence for dinitrogen fixation? *Limnology & Oceanography*, 53(5), 1697–1704. <https://doi.org/10.4319/lo.2008.53.5.1697>
- Pickart, R. S., Nobre, C., Lin, P., Arrigo, K. R., Ashjian, C. J., Berchok, C., et al. (2019). Seasonal to mesoscale variability of water masses and atmospheric conditions in Barrow.
- Pickart, R. S., Pratt, L. J., Torres, D. J., Whittedge, T. E., Proshutinsky, A. Y., Aagaard, K., et al. (2010). Evolution and dynamics of the flow through Herald canyon in the western Chukchi Sea. *Deep Sea Research Part II: Topical Studies in Oceanography*, 57(1–2), 5–26. <https://doi.org/10.1016/j.dsr2.2009.08.002>
- Pierrot, D., Neill, C., Sullivan, K., Castle, R., Wanninkhof, R., Lüger, H., et al. (2009). Recommendations for autonomous underway pCO₂ measuring systems and data-reduction routines. *Deep Sea Research Part II: Topical Studies in Oceanography*, 56(8–10), 512–522. <https://doi.org/10.1016/j.dsr2.2008.12.005>
- Pisareva, M. N., Pickart, R. S., Lin, P., Fratantoni, P. S., & Weingartner, T. J. (2019). On the nature of wind-forced upwelling in Barrow Canyon. *Deep Sea Research Part II: Topical Studies in Oceanography*, 162, 63–78. <https://doi.org/10.1016/j.dsr2.2019.02.002>
- Redfield, A. C. (1958). The biological control of chemical factors in the environment. *American Scientist*, 46(3), 230A–221.
- Rysgaard, S., Glud, R. N., Sejr, M. K., Bendtsen, J., & Christensen, P. B. (2007). Inorganic carbon transport during sea ice growth and decay: A carbon pump in polar seas. *Journal of Geophysical Research*, 112(C3), C03016. <https://doi.org/10.1029/2006jc003572>
- Sato, K., Aoyama, M., & Becker, S. (2010). Reference materials for nutrients in seawater as calibration standard solution to keep comparability for several cruises in the world ocean in 2000s. In M. Aoyama, A. G. Dickson, D. J. Hydes, A. Murata, J. R. Oh, P. Roose, et al. (Eds.), *Comparability of nutrients in the world's ocean* (pp. 43–56). Mother Tank.
- Schlitzer, R. (2016). Quantifying He fluxes from the mantle using multi-tracer data assimilation. *Ocean data view*, 374(2081), 20150288. <https://doi.org/10.1098/rsta.2015.0288>
- Shiozaki, T., Fujiwara, A., Ijichi, M., Harada, N., Nishino, S., Nishi, S., et al. (2018). Diazotroph community structure and the role of nitrogen fixation in the nitrogen cycle in the Chukchi Sea (Western Arctic Ocean). *Limnology & Oceanography*, 63(5), 2191–2205. <https://doi.org/10.1002/lno.10933>

- Sipler, R. E., Gong, D., Baer, S. E., Sanderson, M. P., Roberts, Q. N., Mulholland, M. R., & Bronk, D. A. (2017). Preliminary estimates of the contribution of Arctic nitrogen fixation to the global nitrogen budget. *Limnology and Oceanography Letters*, 2(5), 159–166. <https://doi.org/10.1002/lol2.10046>
- Sommer, U. (1991). A comparison of the Droop and the Monod models of nutrient limited growth applied to natural populations of phytoplankton. *Functional Ecology*, 5(4), 535–544. <https://doi.org/10.2307/2389636>
- Spilling, K., Ylöstalo, P., Simis, S., & Seppälä, J. (2015). Interaction effects of light, temperature and nutrient limitations (N, P and Si) on growth, stoichiometry and photosynthetic parameters of the cold-water diatom *Chaetoceros wighamii*. *PLoS One*, 10(5), e0126308. <https://doi.org/10.1371/journal.pone.0126308>
- Stabeno, P., Kachel, N., Ladd, C., & Woodgate, R. (2018). Flow patterns in the eastern Chukchi Sea: 2010–2015. *Journal of Geophysical Research: Oceans*, 123(2), 1177–1195. <https://doi.org/10.1002/2017jc013135>
- Stroeve, J., & Notz, D. (2018). Changing state of Arctic sea ice across all seasons. *Environmental Research Letters*, 13(10), 103001. <https://doi.org/10.1088/1748-9326/aade56>
- Strong, A. L., Lowry, K. E., Brown, Z. W., Mills, M. M., van Dijken, G. L., Pickart, R. S., et al. (2016). Mass balance estimates of carbon export in different water masses of the Chukchi Sea shelf. *Deep Sea Research Part II: Topical Studies in Oceanography*, 130, 88–99. <https://doi.org/10.1016/j.dsr2.2016.05.003>
- Takahashi, T., Olafsson, J., Goddard, J. G., Chipman, D. W., & Sutherland, S. C. (1993). Seasonal variation of CO₂ and nutrients in the high-latitude surface oceans: A comparative study. *Global Biogeochemical Cycles*, 7(4), 843–878. <https://doi.org/10.1029/93gb02263>
- Takahashi, T., Sutherland, S. C., Wanninkhof, R., Sweeney, C., Feely, R. A., Chipman, D. W., et al. (2009). Climatological mean and decadal change in surface ocean pCO₂, and net sea–air CO₂ flux over the global oceans. *Deep Sea Research Part II: Topical Studies in Oceanography*, 56(8–10), 554–577. <https://doi.org/10.1016/j.dsr2.2008.12.009>
- Thoning, K., Crotwell, A., & Mund, J. (2021). *Atmospheric carbon dioxide dry air mole fractions from continuous measurements at Mauna Loa, Hawaii, Barrow, Alaska, American Samoa and south Pole. 1973-2020*. Version 2021-08-09. National Oceanic and Atmospheric Administration (NOAA). Global Monitoring Laboratory (GML). <https://doi.org/10.15138/yaf1-bk21>
- Tremblay, J. É., Anderson, L. G., Matrai, P., Coupel, P., Bélanger, S., Michel, C., & Reigstad, M. (2015). Global and regional drivers of nutrient supply, primary production and CO₂ drawdown in the changing Arctic Ocean. *Progress in Oceanography*, 139, 171–196. <https://doi.org/10.1016/j.pocean.2015.08.009>
- Tu, Z., Le, C., Bai, Y., Jiang, Z., Wu, Y., Ouyang, Z., et al. (2021). Increase in CO₂ uptake capacity in the Arctic Chukchi Sea during summer revealed by satellite-based estimation. *Geophysical Research Letters*, 48(15), e2021GL093844. <https://doi.org/10.1029/2021gl093844>
- Vernet, M., Matrai, P. A., & Andreassen, I. (1998). Synthesis of particulate and extracellular carbon by phytoplankton at the marginal ice zone in the Barents Sea. *Journal of Geophysical Research*, 103(C1), 1023–1037. <https://doi.org/10.1029/97jc02288>
- von Friesen, L. W., & Riemann, L. (2020). Nitrogen fixation in a changing Arctic Ocean: An overlooked source of nitrogen? *Frontiers in Microbiology*, 11, 3149. <https://doi.org/10.3389/fmicb.2020.596426>
- Wang, H., Lin, P., Pickart, R. S., & Cross, J. N. (2022). Summer surface CO₂ dynamics on the Bering Sea and eastern Chukchi Sea shelves from 1989 to 2019. *Journal of Geophysical Research: Oceans*, 127(1), e2021JC017424. <https://doi.org/10.1029/2021jc017424>
- Wanninkhof, R. (2014). Relationship between wind speed and gas exchange over the ocean revisited. *Limnology and Oceanography: Methods*, 12(6), 351–362. <https://doi.org/10.4319/lom.2014.12.351>
- Weingartner, T., Aagaard, K., Woodgate, R., Danielson, S., Sasaki, Y., & Cavalieri, D. (2005). Circulation on the north central Chukchi Sea shelf. *Deep Sea Research Part II: Topical Studies in Oceanography*, 52(24–26), 3150–3174. <https://doi.org/10.1016/j.dsr2.2005.10.015>
- Weiss, R. (1974). Carbon dioxide in water and seawater: The solubility of a non-ideal gas. *Marine Chemistry*, 2(3), 203–215. [https://doi.org/10.1016/0304-4203\(74\)90015-2](https://doi.org/10.1016/0304-4203(74)90015-2)
- Welschmeyer, N. A. (1994). Fluorometric analysis of chlorophyll a in the presence of chlorophyll b and pheopigments. *Limnology & Oceanography*, 39(8), 1985–1992. <https://doi.org/10.4319/lo.1994.39.8.1985>
- Woodgate, R. A. (2018). Increases in the Pacific inflow to the Arctic from 1990 to 2015, and insights into seasonal trends and driving mechanisms from year-round Bering Strait mooring data. *Progress in Oceanography*, 160, 124–154. <https://doi.org/10.1016/j.pocean.2017.12.007>
- Woodgate, R. A., & Aagaard, K. (2005). Revising the Bering Strait freshwater flux into the Arctic Ocean. *Geophysical Research Letters*, 32(2), L02602. <https://doi.org/10.1029/2004gl021747>
- Woodgate, R. A., & Peralta-Ferriz, C. (2021). Warming and freshening of the Pacific inflow to the Arctic from 1990–2019 implying dramatic shoaling in Pacific winter water ventilation of the Arctic water column. *Geophysical Research Letters*, 48(9), e2021GL092528. <https://doi.org/10.1029/2021gl092528>
- Zehr, J. P., & Capone, D. G. (2020). Changing perspectives in marine nitrogen fixation. *Science*, 368(6492). <https://doi.org/10.1126/science.aay9514>
- Zheng, Z., Wei, H., Luo, X., & Zhao, W. (2021). Mechanisms of persistent high primary production during the growing season in the Chukchi Sea. *Ecosystems*, 24(4), 891–910. <https://doi.org/10.1007/s10021-020-00559-8>
- Zhuang, Y., Jin, H., Chen, J., Ren, J., Zhang, Y., Lan, M., et al. (2020). Phytoplankton community structure at subsurface chlorophyll maxima on the western Arctic shelf: Patterns, causes, and ecological importance. *Journal of Geophysical Research: Biogeosciences*, 125(6), e2019JG005570. <https://doi.org/10.1029/2019jg005570>

References From the Supporting Information

- Anderson, L. G., Jutterström, S., Kaltin, S., Jones, E. P., & Björk, G. (2004). Variability in river runoff distribution in the Eurasian Basin of the Arctic Ocean. *Journal of Geophysical Research*, 109(C1), C01016. <https://doi.org/10.1029/2003jc001773>
- Cooper, L. W., McClelland, J. W., Holmes, R. M., Raymond, P. A., Gibson, J. J., Guay, C. K., & Peterson, B. J. (2008). Flow-weighted values of runoff tracers ($\delta^{18}\text{O}$, DOC, Ba, alkalinity) from the six largest Arctic rivers. *Geophysical Research Letters*, 35(18), L18606. <https://doi.org/10.1029/2008gl035007>
- Guo, L., Cai, Y., Belzile, C., & Macdonald, R. W. (2012). Sources and export fluxes of inorganic and organic carbon and nutrient species from the seasonally ice-covered Yukon River. *Biogeochemistry*, 107(1), 187–206. <https://doi.org/10.1007/s10533-010-9545-z>
- Yamamoto-Kawai, M., McLaughlin, F. A., Carmack, E. C., Nishino, S., & Shimada, K. (2008). Freshwater budget of the Canada Basin, Arctic Ocean, from salinity, $\delta^{18}\text{O}$, and nutrients. *Journal of Geophysical Research: Oceans*, 113(C1).
- Yamamoto-Kawai, M., Tanaka, N., & Pivovarov, S. (2005). Freshwater and brine behaviors in the Arctic Ocean deduced from historical data of $\delta^{18}\text{O}$ and alkalinity (1929–2002 AD). *Journal of Geophysical Research: Oceans*, 110(C10).